Lunds Universitets Naturgeografiska Institution

Seminarieuppsatser Nr. 80

The wind climate of northwestern Europe in SWECLIM regional climate scenarios

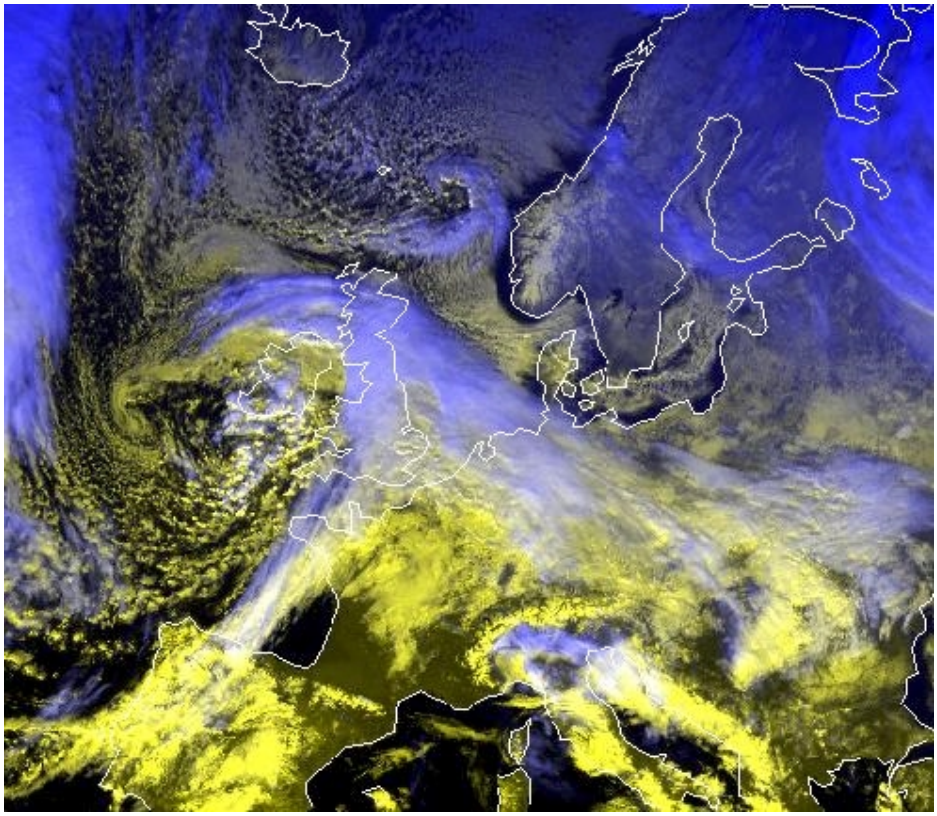

Agneta Andersson

2001

Department of Physical Geography,
Lund University
Sölvegatan 13, S-221 00 Lund,
Sweden

Abstract

The effects of a global climatic change on the wind climate of northwestern Europe are investigated with the aid of a regional climate model. There have up to date been few studies of how the wind climate will react to a greenhouse gas warming. Those that have been done are mostly global scale studies and centered on changes in storm activity during the winter season.

I'm using data from a regional scale model developed by the Swedish Regional Climate Modelling Programme, or SWECLIM. The regional model uses two different global circulation models for boundary conditions (the HadCM2 model and the ECHAM4 model). The data consists of 4-times daily sea level pressure and geostrophic wind speed from a 10-year control and scenario run time slice. The scenario time slice has a 2.5 times higher concentration of CO_2 then the control. I also calculated the wind direction using the modelled geostrophic wind.

I have investigated both the yearly, monthly and seasonal changes and well as changes of the extremes of the wind climate in the form of 95 and 99 percentiles and percentages of windspeed over 20 and 25 m/s.

The model predicts an increased meridional pressure gradient as a result of the greenhouse warming. Regarding the wind climate the model predicts a higher frequency of westerly winds. In the North Sea and the Norwegian Sea there is a small increase of the yearly mean geostrophic wind speed. Sweden and northern Germany also experiences an increase of the yearly mean geostrophic wind speed when running the model with the HadCM2 boundary data, but a decrease when using the other model as boundary conditions. The storm climate shows no major increases in the number of storms per year due to the global warming. What I did find is an increase during autumn in the intensity of storms over the North Sea and the Norwegian Sea. During winter I found a decrease in storm intensity over the same area when using the ECHAM4 model as boundary data. An increase in the intensity of gale winds during autumn was found over Sweden and northern Germany when using HadCM2 boundary data. The ECHAM4 driven model showed a decrease during winter in the intensity of storm and gale winds in this area.

Acknowledgements

I'd like to thank my advisor Dr. Lars Bärring for introducing me to this topic. He's been of invaluable help during this work. I'd also like to thank Markku Rummukainen and Juoni Räisänen for providing the SWECLIM data.

Cover picture: processed Meteosat image. 01-02-07 12:00 (UTC) © 2001 SMHI. From SMHI webpages.

1 Introduction

The possibility of a climate change due to an enhanced greenhouse effect has been the topic of many investigations during the last decade. An increase of the mean global temperature is one of the most discussed effects that are to be expected as a result of climate change. Another possible effect of a climatic change that has recently come to the attention of scientists is a change in the mid-latitude storm activity in the North Sea (IPCC, 1996). Mid-latitude storms might be less intensive than its relatives, the tropical cyclone and the hurricane, but the large areas involved and the large time frame makes the mid-latitude storms just as devastating and economically expensive. Just the two December storms ”Lothar” and ”Martin” in 1999 caused an overall economic loss estimated to EUR 14 bn (Munich Re, 2000). One of the big hazards with these kinds of storms is the danger to boats and coastlines due to the big waves and storm surges generated by the storms. This particularly affects the fishing industry and offshore oil industry among others. The storms themselves are also a big hazard, the winds causing major property damages to buildings and cars and other vehicles, not to mention extensive damage to livestock, agricultural and horticultural products and to forests. The population growth and the growing concentration of people in cities makes mankind more and more vulnerable to natural disasters such as storms. An increase in number or intensity of mid-latitude storminess would lead to an even larger increase of both economical and social damages.

People both within and outside of the scientific community have made a number of reports showing a worsening of the wave and storm climate in the North Atlantic during the last decades. One analysis for example made by Bacon and Carter (1993) showed an increase in mean wave height in the north Atlantic region since 1950. In 1994 a group of scientists started the WASA project (Waves and storms in the North Atlantic) to ”verify or disprove hypotheses of a worsening storm and wave climate in the north-east Atlantic and its adjacent seas in the present century” (The WASA Group, 1998). They found that the wave and storm climate has shown a small increase since the 1960’s, but these numbers are no higher than in the beginning of the century. Similar results were found by Heino et al (1999).

Scenarios on future changes in extra-tropical storm activity under greenhouse warming have been investigated using global circulation models with contradictory conclusions. Zwiers and Kharin (1998) did a simulation with a Canadian GCM under CO_2 doubling. They found a modest reduction of extreme near-surface wind speed in the mid-latitude and tropics and an increase in wind speed over northwestern Europe and at high latitudes. Zhang and Wang (1997) found a reduction in the winter extra tropical cyclone and anticyclone activity under a greenhouse-warming scenario. Lambert (1995) analysed the winter cyclones under CO_2 doubling. He found a decrease in the total number of lows in both the Northern and Southern Hemisphere but an increase in the frequency of intense cyclones. Obviously the results depend on the model used for the analysis.

The purpose of this paper is to analyse the effects of human induced climate change on the future wind climate in a regional climate modelling experiment. The results from a regional impact study are more realistic than compared to the global scale since there are many local effects influencing the wind (i.e. local topography, surface friction etc). Possible causes and effects of changes to the wind climate will be discussed. Both the mean wind climate is examined and if any changes can be found in the storm activity, either in intensity or time distribution. Changes in the extreme of the climate, such as storminess, are often of more importance than the mean climate.

I have used the result, in the form of geostrophic wind and sea level pressure, from a regional circulation model developed by SWECLIM, with boundary conditions from ECHAM4 and HadCM2. SWECLIM (Swedish Regional Climate Modelling Programme) started in 1997 with the purpose to produce regional climate change scenarios for Sweden and the Nordic region. SWECLIM is a joint effort between researches at SMHI and at the universities of Stockholm and Gothenburg (SWECLIM, 1998). More information about SWECLIM can be found on the homepage of SMHI[1]. The data comes from two models that have produced both a control time-slice and a scenario time-slice with a 2.5 times higher concentration of CO_2. The difference between the control and the scenario is the climate change. I have used data from two profiles, one over the North Sea and the Norwegian Sea and the other over Sweden and northern Germany. This gives me the opportunity to find differences between data from over the ocean as opposed to a land surface.

From the model output, the geostrophic wind and the sea level pressure have been used. Geostrophic wind derived from pressure is one of the best tools available for analysing the long-term trend of changes in the storm climate. Geostrophic wind is not affected by local effects and has therefore a closer connection to cyclones/anticyclones. The atmospheric circulation is caused by pressure differences between different regions. Pressure analyses are therefore an important complement to wind analyses, and is needed to understand and explain the processes that control the wind circulation.

2 Background

The surface of tropical and equatorial regions receives a larger amount of solar energy than the Polar Regions on an annual global average. This energy imbalance is compensated for by the atmospheric circulation that along with the oceans redistributes the energy over the globe by transporting energy from the Equator toward the Polar Regions. This chapter gives an overview of the global atmospheric circulation as well as a more detailed one of the mid-latitudes and Europe. I will also address the subject about climate change and give a description of the different climate models used in this work. The major part of this chapter consists of a summary from Henderson-Sellers & Robinson (1994). Other sources of information are explicitly mentioned.

2.1 Air pressure and atmospheric motion

Air movement is caused by variations in the atmospheric air pressure. Air pressure is the force exerted by the weight of a column of air above a certain point on the surface. Air pressure is measured in hPa (hecto Pascal).

The pressure is for most part determined by the density and temperature of the atmosphere. The density and the temperature decreases with height, therefore the pressure also decreases with height. Close to the sea level, an increase in height of 100 m causes a decrease in pressure with around 10 hPa. All pressure observations are therefore reduced to sea level.

[1] www.smhi.se (under the research and development section)

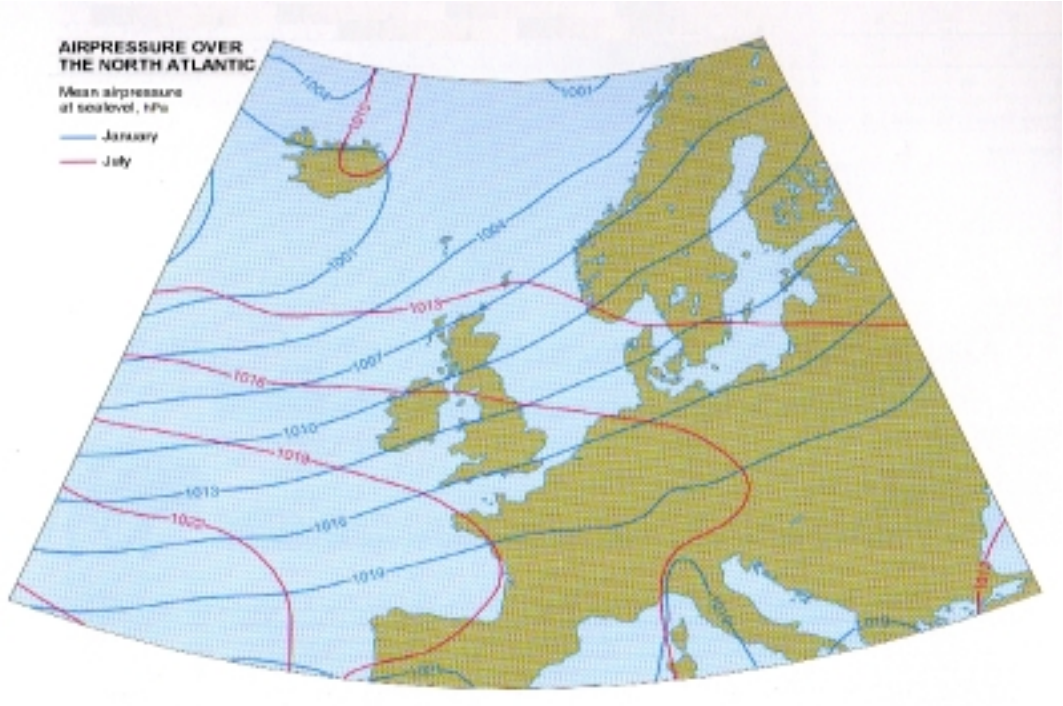

Figure 2.1 Isobar map over the European region for winter and summer (from Skåne atlas).

One way of analysing horizontal pressure variations is to create a pressure or isobaric map. An isobar is a line that connects points with the same pressure. The permanent and semi permanent regions of high and low sea level pressure in winter and summer in the European region can be seen in figure 2.1.

During winter the northern European region is dominated by the Icelandic low-pressure system bringing mild winters with plenty of snow or rain. During summer the Icelandic low becomes less pronounced and the Azores high dominates the region.

The meridional sea level pressure gradient between the Icelandic low and the Azores high is a very useful zonal indice and is known as the North Atlantic Oscillation (or NAO). Other regions in Europe can also be used to define zonal indices. The zonal indice is an indication of the strength of the westerlies, which plays a major role for the climate in Europe. High zonality indicates a strong westerly flow with high cyclonic activity and a strong maritime influence on the climate. Low zonality is an indication of a small latitudinal pressure gradient with a week westerly airflow and a continental influence on the climate (Jacobeit et al, 2001).

The horizontal pressure distribution can also be studied at other atmospheric levels. Here it is best to show the variations in height over a constant pressure surface. This map is similar to the isobaric map, but the lines represent height contours instead of isobars. These height contours can either be in meter (m) or in geopotential meter (a measure of the work required to lift a unit mass from sea level to a height z against the force of gravity (gpm)).

Across the North Atlantic and the North Pacific there are latitudinally confined regions of high eddy activity. These regions are preferred paths for cyclonic activity and are thus called storm tracks. Storm tracks are mostly found during the winter season when cyclonic activity is

highest. Storm tracks are usually identified by a large variation in the bandpass (2-6 days) filtered 500 mb geopotential height field (Hoskins & Valdes, 1990). The two storm tracks in the Northern Hemisphere are the Atlantic storm track and the Pacific storm track. The Atlantic storm track begins in the vicinity of the eastern North America and terminates near the West Coast of Europe. The Pacific stormtrack begins in the vicinity of the eastern Asia and terminates near the west coast of North America (Lau, 1988).

Primarily four different forces acting on the air parcel determine the relative acceleration of an object moving around a rotating planet. These forces are the pressure gradient force, gravitational force, Coriolis force and frictional force.

The pressure gradient force is the force that acts from high to low pressure and is defined as the pressure change over a given distance.

The Coriolis force as is explained by Persson (1998) is caused by the Earth's rotation. If the earth were stationary, an object moving from e.g. north to south above the earth's surface would move parallel with the meridians. However since this is not the case the earth moves taking the meridians and us further east. From our point of view it therefore looks as if the object deviates from its course. A moving object is deflected towards the right by the Coriolis force at the Northern Hemisphere and towards the left at the Southern Hemisphere. The horizontal deviation is largest for horizontal movements at the poles and non-existent at the equator. For vertical movements the vertical deflection is largest at the equator and zero at the poles.

When an object increases its speed, the Coriolis force and with it the deflection increases. This apparent acceleration is called the Coriolis acceleration and is given by:

$$\text{Coriolis acceleration} = (2\Omega \sin\theta)u \qquad (1)$$

Where Ω is the angular rotation rate of the earth, θ is the latitude and u is the speed of the object. $2\Omega \sin\theta$ is called the Coriolis parameter (f) and is constant for given latitude. The magnitude of the Coriolis acceleration varies with the speed of the object as well as with the latitude and acts perpendicular with the direction of the moving object. The Coriolis force is negligible when considering small-scaled wind movements.

2.1.1 Geostrophic wind

In the free atmosphere, about 500-1500 m above the ground, the surface friction has no influence on the wind flow. If the isobars are straight and parallel the pressure gradient force and the Coriolis force are the major forces to influence the wind. When these two forces reach equilibrium a balanced flow, the geostrophic flow is created. It blows parallel with the isobars (figure 2.2) with the low pressure on the left- (right) hand side when you have the wind in your back in the northern- (southern) hemisphere. Because the Coriolis parameter is at or around zero near the equatorial regions the geostrophic wind can't be used in these areas. The speed of the geostrophic wind is proportional to the distance between isobars. The geostrophic wind is a good approximation for the real wind, but it is not a perfect measure. The relation between the geostrophic wind and the true surface wind are influenced by for example stability, gradient winds (explained below) and friction. An approximation of the geostrophic relationship is given by these two equations:

$$u_g = -\frac{1}{\rho f}\frac{\Delta p}{\Delta x} \quad (2)$$

$$-v_g = -\frac{1}{\rho f}\frac{\Delta p}{\Delta y} \quad (3)$$

Where u_g is the west wind component and v_g the south wind component, f is the Coriolis parameter, ρ the air density and $\Delta p/\Delta x$ and $\Delta p/\Delta y$ is the pressure gradient per unit distance in the x (north) and y (east) direction respectively.

The geostrophic wind speed (V_g) can than be calculated using the vectors above (Stull, 1995):

$$V_g = \left[u_g^{\,2} + v_g^{\,2}\right]^{1/2} \quad (4)$$

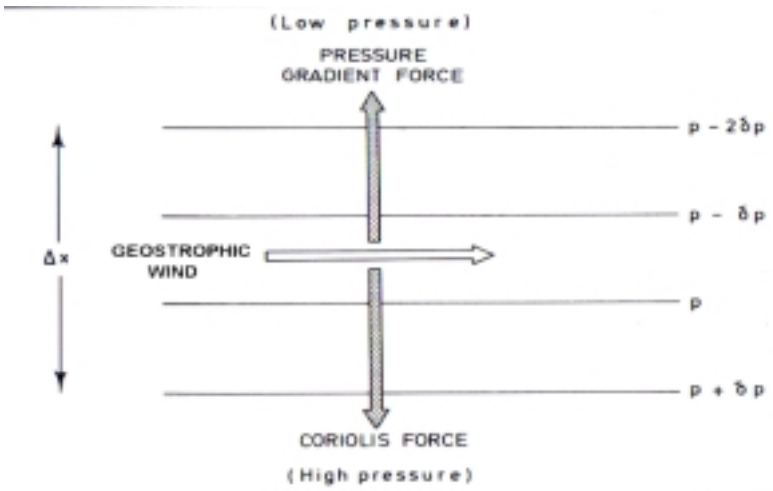

Figure 2.2 The geostrophic wind balance between the pressure gradient and the Coriolis force (from Henderson-Sellers & Robinson, 1994)

2.1.2 Gradient wind

The geostrophic wind relationship is only valid when the isobars are straight and parallel. When the isobars are curved a third force comes into work, the centrifugal force. This acts out from the centre in all curved movements. During rotation around a high-pressure centre this force tends to work in the same direction as the pressure gradient force and acts to speed up the wind compared to the geostrophic wind. Around a low-pressure centre the centrifugal force acts in the opposite direction compared to the pressure gradient force and slows down the wind to below the wind speed of the geostrophic wind. But because low-pressure centres allow for larger pressure gradients and therefore higher wind speeds than high-pressure centres, storms are associated with low-pressure centres (Stull, 1995). The resulting wind that develops when the centrifugal, the pressure gradient and the Coriolis forces are in balance is

called the gradient wind. The direction of this wind is the same as the geostrophic wind, parallel to the isobars. The difference in speed between the geostrophic wind and the gradient wind is greatest with strong curves and large pressure differences.

2.1.3 Ageostrophic wind

Close to the ground the winds moving over obstacles on the earth's surface are affected by friction. The frictional force acts against the direction of the wind movement and reduces the wind speed, by transferring momentum from the air to the ground. The reduced wind speed lowers the Coriolis force, which depends on the wind speed. An ageostrophic flow that crosses the isobars towards lower pressure develops. The angle at which the wind crosses the isobars depends on the magnitude of the frictional force, which is largest at the ground and decreases with altitude.

2.1.4 Barotropic and baroclinic atmosphere

Since pressure and temperature varies with altitude horizontal winds also exhibits vertical variations. A warm air layer has a lower density than a cold air layer; the height differences between two pressure levels are therefore larger in the warmer air layer.

In a barotropic atmosphere there are no horizontal temperature gradients, i.e. the temperature along an isobaric surface is constant, and the density of the air layer only depends on the pressure. There is therefore no spatial change of the air layer thickness and consequently no change in the wind speed or direction with altitude, meaning no disturbances in the air layer.

In an equivalent barotropic atmosphere there exists a horizontal temperature gradient where the isotherms are parallel with the isobars. This thermal gradient causes a change of the wind speed with height, but no change in wind direction and therefore cannot create any disturbances. The vector difference between the geostrophic winds at two different levels is called thermal wind. This wind is very useful. If the geostrophic wind at a specific pressure is known along with the mean horizontal temperature gradient in the layer, the thermal wind can be used to calculate the geostrophic wind at another pressure level.

In a baroclinic atmosphere the density depends on both the pressure and temperature. The temperature varies independently of the isobars, causing the wind speed and direction to vary with altitude. This causes disturbances in the wind flow. The thermal wind blows parallel with the isotherms. Its speed is proportional to the spacing of the isotherms and it blows, in the Northern Hemisphere, with the low temperature to the left. Since the isotherms crosses the isobar advection of energy results. In the Northern Hemisphere a geostrophic wind turning clockwise (anticlockwise) with altitude is associated with a cold air (warm air) advection. In the Southern Hemisphere the conditions are reversed.

2.2 Atmospheric circulation of the mid-latitudes

The atmospheric circulation of the mid-latitudes is dominated by the prevailing westerlies. In a narrow band a major poleward temperature gradient can be found. This area is commonly known as the polar front. The large temperature gradients in this region provide perfect conditions for development of baroclinic conditions. At the polar front there is an increase of wind speed with height leading to the development of a jet stream just below the tropopause. The jet stream is a belt of very fast moving winds, a few kilometres wide, hundreds, or even thousands, of kilometres long and a depth of a few hundred meters. The polar front and its associated large temperature gradient influences the tropospheric westerly wind flow, creating a wave like wind pattern known as Rossby waves. These waves are one of the most important features of the mid-latitude circulation. The Rossby waves cover most of the midlatitudes but are best developed in the narrow band were the polar front is located.

The amplitude of a Rossby wave changes in an almost cyclic like pattern with a period of 20-60 days. The amplitude is characterised as an index. The index is defined as the pressure difference between two latitudes; in the Northern Hemisphere these latitudes are normally chosen between 35°N and 55°N. During a high index circulation there is a strong zonal flow and a number of relatively smooth Rossby waves. When the index decreases the amplitude increases and distinctive large-scale low and high-pressure centres are formed. When the index changes from low to high a blocking anticyclone or a non-frontal depression may occur.

2.2.1 Cyclones and anticyclones

Frontal cyclones

A cyclone (or depression) is a low-pressure centre with an anticlockwise (clockwise) air circulation around its centre in the Northern (Southern) Hemisphere. Near the ground the air around a cyclone tends to converge toward its centre causing a rising of air and a tendency for cloud formation. A frontal cyclone develops along a front, a front being a region with a marked horizontal temperature gradient, like for example the polar front. The birth and intensification of a cyclone is called cyclogenesis.

According to the classic model of depression development produced by the ’Bergen school’ of meteorologists a cyclone is developed along a front in 6 different stages, which can be seen in figure 2.3. The warmer air along the front rises and is replaced by converging air in the lower troposphere. A low pressure is formed and the air starts to rotate cyclonically. The pressure falls, because the divergence in the upper troposphere removes the air from the depression faster than the convergence replaces the air in the lower troposphere. The depression continues to deepen and the amplitude of the frontal wave gets bigger. The cold air moves faster than the warm air, this causes the warm sector to shrink until the cold air mass takes over the warm air mass and occlusion takes place (stage E). After the occlusion the depression loses the temperature contrast. The cyclonic circulation can be maintained for a few days but sooner or later the winds will die down. The whole sequence of cyclone development can take about a week, during which the cyclone may have moved two or three thousand kilometres eastward. Several cyclones, usually around three or four, can form after one another, creating a family of depressions.

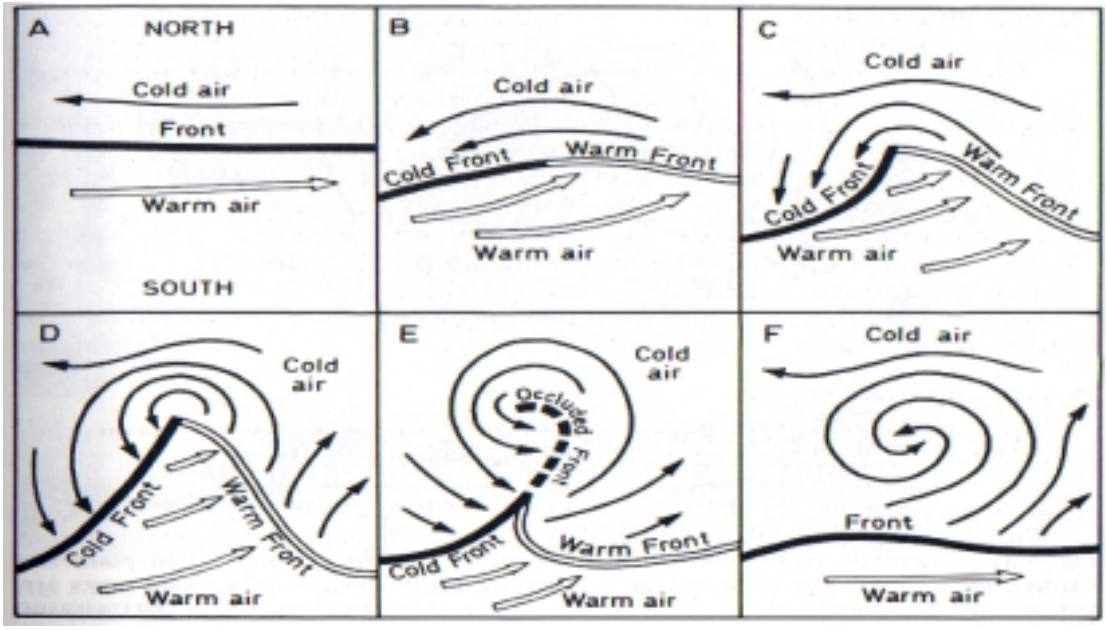

Figure 2.3 The different stages of cyclone development, from the initial state to the occlusion. (Henderson-Sellers and Robinson, 1994)

Anticyclones

An anticyclone is a centre of high surface pressure with air spiralling clockwise in the Northern Hemisphere and anticlockwise in the Southern Hemisphere. An anticyclone is a region of descending air and divergence at the surface, giving generally clear sky conditions. There are several classes of anticyclones. The travelling anticyclones occur between members of a depression family, giving rise to clear weather between the passages of depressions. Blocking anticyclones develops as a result of the index cycle of the Rossby wave (ch. 2.2). These can greatly influence the weather over North Western Europe, giving nice and warm weather persisting for several weeks, forcing the depressions to take a more northerly route.

2.3 Climatic change

2.3.1 Cause

The energy the earth receives from the sun is the main source for the atmospheric energy transport that gives us our climate. But were it not for the atmosphere and its greenhouse effect the mean surface temperature on earth would be more than 30°C below that of today. Jones et al (1999) did a study of the changes in surface air temperature during the last 150 years. They found the annual average global surface temperature during 1961 – 1990 to be 14°C. The mean surface temperature was found to be higher in the Northern Hemisphere (14.6°C) than in the Southern Hemisphere (13.4°C). The so-called greenhouse gases (mainly H_2O (g), CO_2, CH_4, N_2O, CFC's and O_3) absorb some of the earth's emitted thermal radiation and radiate it back to earth, thereby keeping the heat from escaping the atmosphere. This

process is known as the atmospheric greenhouse effect. Changes in any factor that alters the radiation emitted from earth or received from the sun, or which changes the redistribution of energy around the globe can have an affect on the climate. An increase in the concentration of greenhouse gases will lead to a more efficient greenhouse effect. More of the emitted long wave radiation will be prevented from escaping the atmosphere leading to a warming of the lower atmosphere and surface. This is the enhanced greenhouse effect.

Changes in the climate can be divided into two different groups. Natural causes or anthropogenic causes (climate change caused by human activity). Natural processes that can lead to global scale changes in the climate are divided into external and internal processes. External changes are caused by alterations of the processes outside of the climate system. For example changes in earth's orbit around the sun. These changes lead to very long-term changes in the climate system, in the order of 100.000 years or more. The internal processes that can cause changes in our climate are for instance volcanic eruptions. Volcanic activity releases aerosols into the atmosphere along with water vapour and carbon dioxide. Aerosols (tiny liquid and solid particles) scatter and absorb radiation and tend to cool the surface. The energy and type of volcanic eruption mostly determine the climate change, which is rather short lived (a few years) and results in a temperature anomaly of a few tenths of a degree. Other natural internal factors are the amount of dust in the atmosphere, the reflectivity of the ice sheets, concentration of greenhouse gases, changing characteristics of clouds (see anthropogenic causes below) and rebounding of land, having been depressed by ice among others (IPCC, 1996).

During the industrial era there has been a measurable increase in greenhouse gases and aerosols that is believed to be due to human activity. For example the burning of fossil fuels and deforestation of tropical rain forests releases carbon dioxide into the atmosphere. This increase in CO_2 strengthens the greenhouse effect. Aerosols are also released by human activity, such as production of fossil fuel and biomass burning. Methane has also increased since the pre-industrial level. Methane emissions from anthropogenic emissions contribute between 60-80% of the global emissions (IPCC, 1996).

2.3.2 Effects

A problem when considering the effects of climatic change is the internal interactions in the climate system, the so-called feedback mechanisms. The feedback can work in both a positive and a negative direction. One example of a positive feedback is when the temperature rises leading to higher evaporation. The higher concentration of water vapour in the atmosphere leads to an increased absorption of the earth's infrared energy. This causes a further increase in temperatures. Another positive feedback is the ice-albedo feedback mechanism. A higher temperature melts more ice and snow in the polar latitudes. This reduces the surface albedo (reflectivity) why more solar energy reaches the surface leading to higher temperatures. The feedback involved with increasing cloudiness because of increased evaporation caused by higher temperatures is less understood. An increase in low and middle clouds is believed to produce a negative feedback slowing the warming. This is because the increased cloudiness will reflect more incoming solar energy. An increase in cirrus clouds (high clouds) on the other hand have a smaller impact on the albedo and is expected to lead to a positive feedback because the increase in water vapour will enhance the greenhouse effect. Because of the large impact clouds has on the radiation budget and hydrological cycle, this lack of understanding regarding cloud-related feedback is a major source of uncertainty in climate modelling.

There is evidence showing that the mean global surface temperature has increased since the late 19th century by about 0.3 – 0.6°C. The latest 40 years shows a slower warming trend, about 0.2 – 0.3°C. The temperature in the stratosphere as opposed to the surface has decreased by 0.6°C between 1979-1994 (IPCC, 1996). It is argued among scientists if the global warming is a result of anthropogenic forcing or just a part of nature's variability (e.g. Corti et al., 1999). The global surface warming has not been uniform over the globe. The continents between 40°N and 70°N have exhibited the greatest warming. Some areas have actually cooled in recent decades, for example the North Atlantic Ocean north of 30°N. Globally the continents have experienced greater warming than the oceans, creating an increased thermal gradient between land and ocean.

Finding long-term changes in the wind climate is not an easy task. The difficulty lies in finding a good set of reliable wind observations. Wind has only been measured the last half of the 19th century and these data series are often not homogenous. Earlier analysis was subject to estimation using the Beaufort scale. Here the wind is classified into 13 different classes (0-12), depending on for example wave height and visibility or on land how much trees move in the wind or how much damage they do (Korevaar, 1990). A few analyses have used data of storm surges and waves. Bacon and Carter (1991) found an increase in mean wave height over the North Atlantic region since around 1950 when analysing the long-term trend in the wave climate of North Atlantic and North Sea using both visual estimates and instrumental measurements of wave height. Von Storch and Reichardt (1997) analysed past variations of water levels at Cuxhaven, Germany, but found no significant increase of storm-related water levels in the past. Kushnir et al (1997) used twice daily surface wind observations from 1980-89 to generate a monthly averaged significant wave height history. They used a canonical correlation analysis to find a link between the significant wave height and the monthly averaged sea level pressure data. This link was then used to generate an extended statistical hindcast of monthly mean wave fields from 1960 and onward. They found an increasing trend in significant wave heights at several locations in the northest Atlantic.

Earlier analysis has instead of wind observations used pressure data in various ways. Using calculated percentiles of surface geostrophic winds derived from triangles of stations with air pressure observations over north-western Europe, Alexandersson et al (1998, 2000) found a small increase in storm activity since the 1960s, this increase being more pronounced over the maritime areas. But these values correspond with values from the beginning of the century. Schmidt & von Storch (1993) on the other hand found no changes in the storm statistics in the past 100 years, when analysing the geostrophic wind calculated from sea level pressure measurements at 3 different locations in the German bight. Schmith et al (1998) used observed sea level pressure from 8 stations in the Northeast Atlantic for the period 1875-1995. They calculated 24-hour tendencies (the absolute 24-hour change in pressure) by applying a high-pass filter. They found a small increase in winter storminess during the past 2-3 decades in the northeast Atlantic.

2.3.3 Modelled future changes

Model based predictions of future climate change depend on the scenario used to force the model. Of the different scenarios used in IPCC (1996) all of them show the same trend of a global mean temperature increase and a global mean sea level rise by 2100. When taking into account all the different scenarios, the increase in global mean temperature varies between 0.9

and 3.5°C and the global sea level rise between 13 and 94 cm. The above-mentioned rise in global sea level and temperature along with an increased precipitation in high latitudes in winter is a common feature in all model simulations, but the modelled global warming is not uniform over the globe, neither in time nor in space. The warming is greater in Polar Regions than in the tropics. The warming is also greater over continents than over oceans and greater in winter than in summer.

The changes in mid-latitude storminess under greenhouse warming are more uncertain. The north to south temperature gradient is one of the main energy sources for mid-latitude depressions together with the latent heat released during water vapour condensation. Because the high latitudes experience the greatest warming, this means that the meridional temperature gradient will decrease. A decrease in the polar-equator temperature gradient along the polar front will lead to a decreased baroclinicity; this should weaken the intensity of mid-latitude storms. On the other hand the increased baroclinicity above, because of an increased meridian temperature gradient in the upper troposphere, is associated with an increase in mid-latitude storm activity (Carnell & Senior, 1998). The results of a $2\times CO_2$ time-slice experiment done by Beersma et al (1997) suggests that the effects of an increase in the upper troposphere temperature gradient approximately balances the effects of the decrease in the lower troposphere temperature gradient, giving a small net effect on mid-latitude storminess.

In the case of a global warming, evaporation will increase leading to a rise in the atmospheric water vapour content. This could influence the extra-tropical storminess in different ways, either to an intensification of extra-tropical storms or to a decrease in the extra-tropical storm activity (e.g. Zhang & Wang, 1997). An increase in water vapour concentrations in the lower troposphere means that there is more moisture available for condensation in extra-tropical low-pressure systems. This will increase the release of latent energy in the atmosphere and thus enhance the potential to kinetic energy conversion. This will intensify the extra-tropical storms. On the other hand because the increased water vapour concentration is larger in low latitudes, the meridianal transfer of moisture increases. The increase in moisture content in high latitudes leads to an enhancement of the latent heat release, which weakens the meridian temperature gradient and thereby reducing the extra-tropical storm activity.

Carnell and Senior (1998) modelled the intra-seasonal variability in Northern Hemisphere winter using the HadCM2 model. They found a reduction in the total number of storms in the source regions in both the North Atlantic and North Pacific, due to an increase in local diabatic heating. Their result suggested that the increase in water vapour concentration be of more importance for changes in storm activity than a reduction of the meridional temperature gradient.

2.4 Climate modelling

2.4.1 Global climate models

A climate model is a simplified mathematical representation of all the processes that control the climate. Some of the most important processes when constructing a climate model include radiation processes, the energy balance and the difference between land/ocean/ice surfaces. These processes are complex and not fully understood. The generalisation of these processes is generally made in two different ways. The first is a simplification of the processes themselves. This can be approached empirically, by using available observational data or

theoretically, by specification of the physical laws involved. The second way involves the time and space resolution. Both these resolutions depend on data and computational availability as well as model design. The higher the time and spatial resolution is, the more reliable the results.

A computer model starts with the present or pre-industrial conditions and then studies the effects of changing one or more component of the climate system. The computational procedure for reaching the required results often uses a time-step approach, meaning that the processes runs for a specific length of time after which new conditions are calculated and the process is repeated with the new conditions. Before using the model results for predicting future climate change, it is first tested by comparing it to the present climate. There will always be inherent uncertainties in the result because of insufficient observational data for the starting conditions and incomplete description of the physical processes.

A general circulation model, or GCM for short, is a full three-dimensional model that represents most of the important physical processes. They incorporate mathematical descriptions of the atmosphere as well as oceans, land, biosphere and cryosphere. In a GCM the earth's surface is divided into a series of rectangles called grid points. In the vertical the atmosphere is divided into approximately 6-10 levels, these levels are usually specified as constant pressure surfaces. The starting conditions are specified at each grid point as well as each level in the vertical. The equations are solved using the time-step approach and the results are interpolated between grid points.

Because the thermal capacity of water is so much greater than air, the oceans play a very important role in distributing energy and moisture from the tropics to the poles. The oceans are also a major sink of heat, carbon and CO_2. A GCM that has incorporated a three dimensional representation of the oceans into the model are called a coupled ocean-atmosphere global circulation model, or OAGCM for short. OAGCM's are physically more realistic for projecting future climate changes, especially the timing of the changes as well as the regional distribution. An important aspect of OAGCM's is that they also offer the possibility of taking into account various feedback mechanisms, which is essential for climate change modelling. OAGCM's are therefore the best tool available today for simulating future global climate change.

When running a coupled ocean-atmosphere model it is often necessary to adjust or "spin up" the atmosphere and ocean to a stable mutual equilibrium before starting any climate change studies. This is done to achieve negligible climate drift in the control run.

The HadCM2 model

HadCM2 (Hadley Centre Coupled Model, version 2) is a coupled OAGCM developed at the Hadley centre in UK. A detailed description of this model is given by Johns et al (1996) and a summary follows.

HadCM2 has a horizontal resolution of 2.5 degrees in latitude by 3.75 degrees in longitude. The vertical resolution of the atmosphere is 19 levels in hybrid co-ordinates. This puts surface pressure and thermodynamic variables at the centre of the grid cell and the wind components at the corners. The atmosphere uses a 30-minute time step for most computations except radiation. The radiation scheme uses 4 spectral bands in the short wave and 6 spectral bands

in the long wave calculations. Radiation calculations take into account the radiative effects of clouds and trace gases (water vapour, carbon dioxide and ozone). Albedos over ocean surfaces differentiate between bare ice and snow covered ice. Over land the albedo depends on if the surface is snow-free or snow-covered and the vegetation type. For calculations of soil temperatures the model uses a 4-layer model imbedded in the land surface. This gives greater accuracy for diurnal and seasonal soil temperature cycles. The surface hydrology includes ground storage, storage in vegetative canopy, river outflow, and surface and sub-surface runoff.

The ocean component of the model has a vertical resolution of 20 depth levels and a time-step of 1 hour. Both the vertical mixing and horizontal diffusivity is calculated in the energy balance mixed layer model. The coupling cycle of the ocean and atmosphere consists of a one-day cycle.

To bring the model to equilibrium a coupled spin up was used. The model was spun up for 510 years and not to full equilibrium because of computational economy. The control run for the climate change study started after the 510-year spin up. The anomaly runs was then started 10-years after the control (~1860). The first 10 years of the control run are neglected because of adjustments of the model from the spin up phase. The difference between the control and anomaly run is the climate change since pre-industrial climate.

The ECHAM4 model

ECHAM4 is a coupled OAGCM that has been developed at the Max Planck Institute für Meteorologie in Hamburg and has evolved from a spectral numerical weather forecasting model by the European Centre for Medium Range Weather Forecasts (ECMWF). The prognostic variables include vorticity, divergence, temperature, surface pressure, cloud water and water vapour (Chen & Roeckner, 1996).

The horizontal resolution of the model is T42, which corresponds to about 2.8 degrees in latitude by 2.8 degrees in longitude. The vertical resolution is 19 levels in hybrid sigma-pressure co-ordinates, with the top at 10hPa. For the atmosphere the model uses a time step of 30 minutes for dynamics and physics. For radiation the time step is 2 hours. The radiation scheme uses only 2 bands in the short wave spectrum, the first band has the spectral interval of 0.25-0.68μm and the second band 0.68-4.0μm. The long wave spectrum is divided into 6 bands. The radiation scheme takes into account the radiation properties of several greenhouse gases, such as water vapour, carbon dioxide, ozone, methane, nitrous oxide, 16 CFC's and various types of aerosols. For the cloud and moisture advection a semi-Langrangian transport method is used (Chen & Roeckner, 1996).

2.4.2 Regional climate models

The global coverage and the long time series prevent the GCM's from being run at a high resolution. For regional impact studies it is therefore necessary to downscale to a higher spatial resolution. The regional climate model (or RegCM for short) takes into account local effects on the climate such as mountains, lakes and other surface physiographies. There are several different techniques for downscaling GCM's. Statistical downscaling is a method that develops statistical relationships between local and large-scale climate variables. These

relations are then applied to the output of GCM simulations. The dynamical downscaling interprets the time dependant physical interactions between the global and the regional climate. The technique of using output data from GCM simulations, as initial and driving lateral meteorological boundary conditions for the RegCM simulations, are called one-way nesting modelling (e.g. Giorgio (1990) & Giorgio et al (1994)). It is one-way because the local conditions in the high-resolution model are not fed back to the GCM.

RCA

RCA, the Rossby Centre regional Atmospheric climate model, is a regional downscaling for Scandinavia. The Rossby centre at SMHI has developed RCA as a part of SWECLIM (Swedish Regional Climate Modelling Programme). RCA builds on the limited area model HIRLAM, which is used for weather forecasting. A description of the first version of the model is given by Rummukainen et al (1998). The version used in this work has a resolution of 88 km compared to 44 km in the first version. The first multi year simulation with the regional climate model (RCA) was run in 1998 with HadCM2-boundary data. In 1999 they also started using ECHAM4-boundary data.

3 Material and Methods

This chapter gives a brief overview of the material used along with a description of the analyses done to achieve the purpose of this work as outlined in the Introduction. A more in depth description of the regional climate model and the two GCM's used for boundary conditions were given in the chapters above (2.4.1 and 2.4.2).

3.1 Data

The analysed data consists of geostrophic wind and the sea level pressure (slp) from the RCA model. The RCA model runs have been forced with boundary data from both the HadCM2 model and the ECHAM4 model. The first run uses HadCM2 boundary data with a 10-year control run and a 10-year scenario run. The other run uses ECHAM4 boundary data with a 10-year control run and a 10-year scenario run.

The control run of the HadCM2 model is run with the pre-industrial level of greenhouse gases. The scenario run of the HadCM2 model is run with an increase in greenhouse gas concentration according to measurements from 1860-1990 and 1-percent increase after 1990. Both the control and scenario run of the HadCM2 model extends from 1860-2100. The RCA is forced with a time slice, extending from 2039-2049, from the HadCM2 control and scenario runs. This is illustrated in figure 3.1. In the HadCM2 scenario run time slice the greenhouse gas concentration is 2.5 times higher and the global mean temperature 2.6°C warmer compared to the control time slice. If one takes these values and projects them from the present (the control run equals the pre-industrial level and not the present) into the future, these values would equal the IPCC's estimate for approximately the year 2100. (Rummukainen et al, 1998).

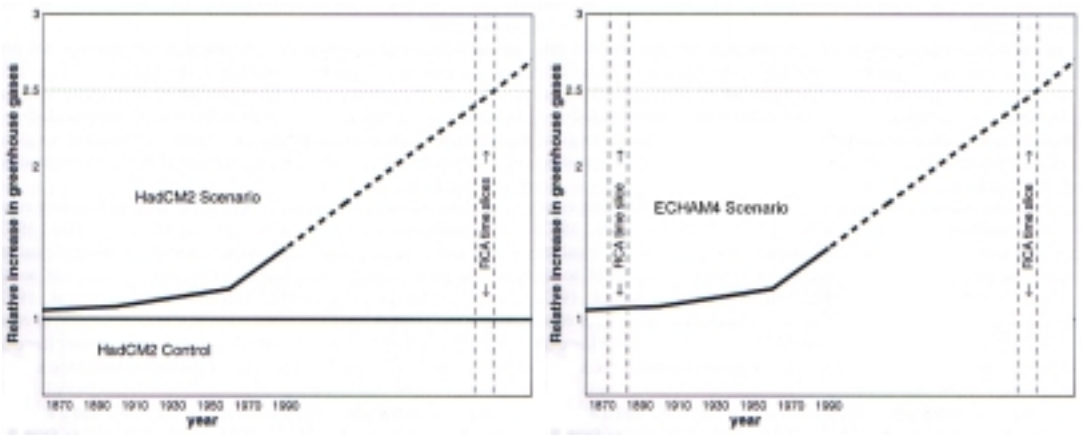

Figure 3.1 a (left) and b (right) show the time-slices from the scenario and control run for HadCM2 (a) and for ECHAM4 (b) (Rummukainen et al, 1998)

ECHAM4 has a scenario run but no control run. Instead the 10-year time slice for the RCA control run was taken from the beginning of the ECHAM4 scenario run before the increase in greenhouse gases. Figure 3.1 b) is a figure that has been manipulated from figure 3.1 a) in an attempt to show this.

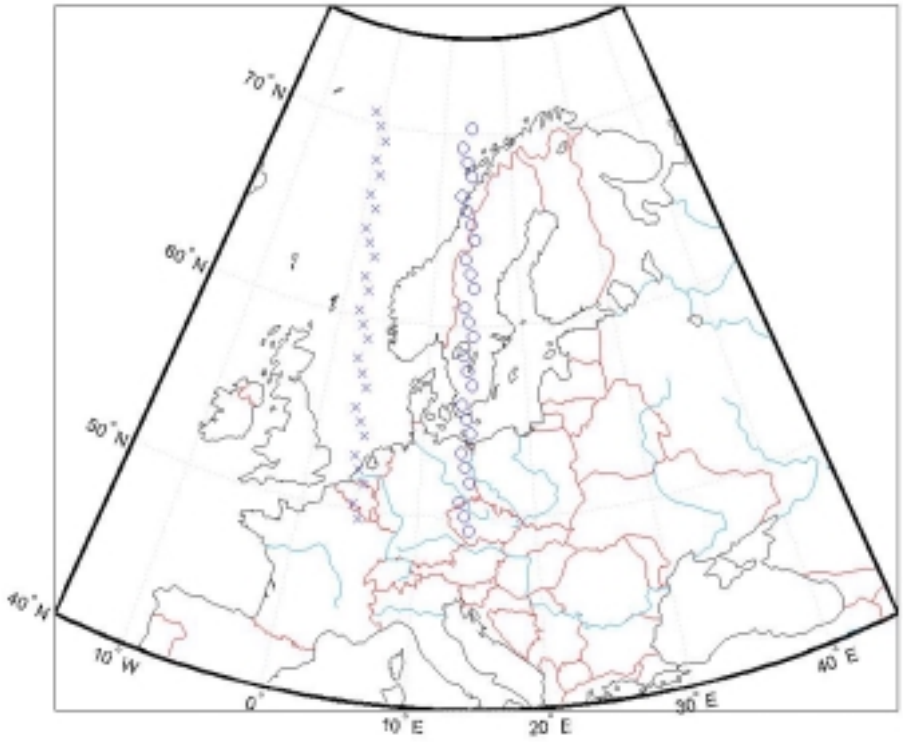

Figure 3.2 Map showing the location of the grid points in the North Sea profile (x) and the Swedish profile (o).

I chose to extract data for two different profiles. Each profile contains 26 grid points from north (grid point 26) to south (grid point 1). The first profile goes through the Norwegian Sea and then down through the North sea (Ns for short), the other through Sweden and down through Germany (Sw for short). Figure 3.2 shows the position of the grid points in a map over Europe. The co-ordinates in lat/long for each grid point can be found in appendix I. Each grid point contains data from 4 times per day at a 6-hour interval starting at 00UTC Dec01, year 0 to 18UTC Nov30, year 10. Each month is exactly 30 days long. The grid points have a resolution of 88km.

3.2 Analyses

In all analyses, a study of the climate change has been made as well as a comparison between and also within the North Sea and the Swedish profiles. Also the different results resulting from the use of the HadCM2 model versus the ECHAM4 model as boundary conditions have been examined. The software that has been used for the analysis is Matlab (student version). Minitab 12.21 has been used for the statistics. Matlab and also Excel have been used for making graphs.

The resultant geostrophic wind vector and the wind direction were calculated from the westerly and southerly geostrophic wind components (equation 4). The changes in wind direction were analysed for 3 different areas of the profile. These areas were selected based on their position in the profile. The northern most area is in the middle of the Nowegian Sea in the Ns profile (mean of grid points 19-21) and on the Norwegian coast in the Sw profile (mean of grid points 20-22). The middle most area is off the Norwegian coast in the Ns profile (mean of grid points 12-14) and in the middle of Sweden in the Sw profile (mean of grid points 13-15). The southern most area is situated between England and Denmark in the Ns profile (mean of grid points 6-8) and around Skåne in the Sw profile (mean of grid points 7-9).

The yearly mean and the monthly mean of the geostrophic wind and the sea level pressure were analysed in order to get an overview of the effects of the atmospheric greenhouse effect on the seasonal and yearly variations. The seasonal variation was the first to be analysed by calculating one mean value per month and decade for all 26 grid points. This monthly mean value was then subtracted from each grid point for each respective month for the whole 10-year period. This anomaly value makes it easier to analyse the differences within the profile without interference from the natural seasonal variability. The yearly mean was analysed by calculating one yearly mean value for each year and profile.

The zonality is the difference in pressure between the northern and the southern most grid points (the difference between the mean pressure of grid points 24-26 and 1-3). The zonality was calculated separately for each season, winter (Dec-Feb), spring (March-May), summer (June-Aug) and autumn (Sep-Nov).

Also the grid point pattern of the frequency of lowest pressure was examined. For each observation (4 times per day) the grid point that has the lowest pressure was found. The frequency of lowest pressure for each grid point during the decade was then calculated as well as the frequencies of lowest pressure during summers and winters respectively. A comparison between control and scenario run makes it possible to analyse the changes in the regional atmospheric pressure distribution due to an enhanced greenhouse effect.

To study changes in the intensity of the storm climate the 95 and 99 percentiles of the geostrophic wind was calculated. Both the yearly mean as well as the monthly mean of the percentiles was examined. The percentage of wind speeds above 20 and 25 m/s was also investigated to look for seasonal changes in storminess and in the intensity of strong winds. A wind speed of 20 m/s is a wind strength of 8 (17.2 – 20.7 m/s) in the Beaufort wind scale which represent a gale wind. 25 m/s is a wind strength of 10 (24.5 – 28.4 m/s), which is the lowest boundary for storm winds (Korevaar, 1990). The percentage of winds above these values was calculated separately for each season- winter, spring, summer and autumn.

To discover the atmospheric greenhouse effect on the geostrophic wind speed, the climatic change, in other words the control minus the scenario run, was calculated. Both the monthly mean and the yearly mean of the climate change were calculated.

3.2.1 Statistics

A balanced ANOVA (a variance analysis) was calculated on the monthly mean values for both the geostrophic wind and the sea level pressure in order to find any statistical differences between the scenario and the control runs. Differences between the two profiles (Sweden and the North Sea) were also checked as well as difference between the runs forced with data from the HadCM2 model and the ECHAM4 model. Because of the large amount of data being analysed, the variance analysis was made on the monthly mean values of three selected areas of the profile. These areas are the same as for the wind direction analysis. For the Ns profile the three selected areas are the mean of grid points 19-21, 12-14 and 6-8. For the Sw profile the mean of grid points 20-22, 13-15 and 7-9 was used.

4 Result

4.1 Sea level pressure

4.1.1 Yearly mean

A clear trend in figure 4.1 is that the yearly mean value is lower in the scenario run than in the control run. The difference in the yearly mean value between scenario and control runs averaged over the whole decade in the 8 boxplots varies between 0.3 to 0.7 hPa. The run using ECHAM4 boundary data (ECHAM4 run) clearly shows higher yearly values than the run using HadCM2 boundary data (HadCM2 run). The standard deviation for the ECHAM4 runs varies between 0.75 and 1.67 hPa compared to between 0.82 and 1.23 hPa for the HadCM2 run. Also the control for the ECHAM4 runs has a higher standard deviation than the scenario, the opposite is true for the HadCM2 runs.

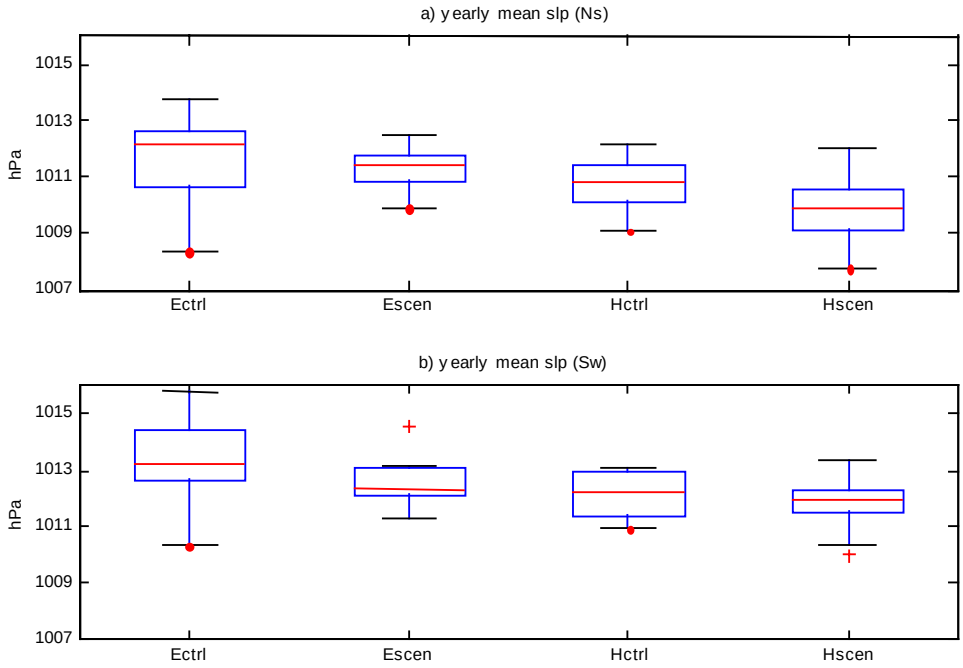

Figure 4.1 Yearly mean sea level pressure for the North Sea (a) and the Swedish (b) profile.

Next a test was carried out to find any statistically significant differences between the scenario run and the control run. The variance was tested using an F-test. A difference in variance was found between the scenario and control run in the ECHAM4 runs for both profiles; a 2-sample T-test was used for these runs. For the HadCM2 runs in both profiles no difference in variance was found and a Mann-Whitney test (a non-parametric test of the medians of two samples) was used instead. The resulting p-values can be seen in table 4.1 and 4.2. No significant difference between the control and scenario runs could be found.

Table 4.1 p-values from the Mann-Whitney test at alpha = 0.05

	p-value
HadCM2 Ns	0.211
HadCM2 Sw	0.570

Table 4.2 p-values from the 2-sample T-test

	p-value
ECHAM4 Ns	0.52
ECHAM4 Sw	0.33

4.1.2 Monthly mean

In both control runs for the Ns profile (figure 4.2 and 4.3) the seasonal variation is very distinct with its highest pressure in summer (April-July) and lowest pressure in winter (Nov-Feb). In the two scenario runs this trend is still visible but not as distinct. In the Sw profile (figure 4.4 and 4.5) the seasonal distribution shows more variation in both the control and scenario runs. Only the HadCM2 control run shows any seasonal distribution, with the highest pressure in summer (April-June) and lowest pressure in winter (Nov-Feb). One common factor in the monthly mean for both the Ns and Sw profile is that the scenario runs all have lower yearly mean pressure value (the difference is less than 1 hPa) than the control run (see the dashed lines in figures 4.2-4.5). The Sw profile has a higher mean pressure value than the Ns profile, in the order of 1-2 hPa. The anomalies (figures c) and d) in figure 4.2-4.5) all shows the highest anomalies in the southern most grid points, especially during winter and spring and the largest negative anomalies in the northern most grid points. In other words the southern most grid points have higher monthly mean pressure than the northern most grid points. The pressure difference between Ns and Sw is largest in winter and spring, and lowest in summer.

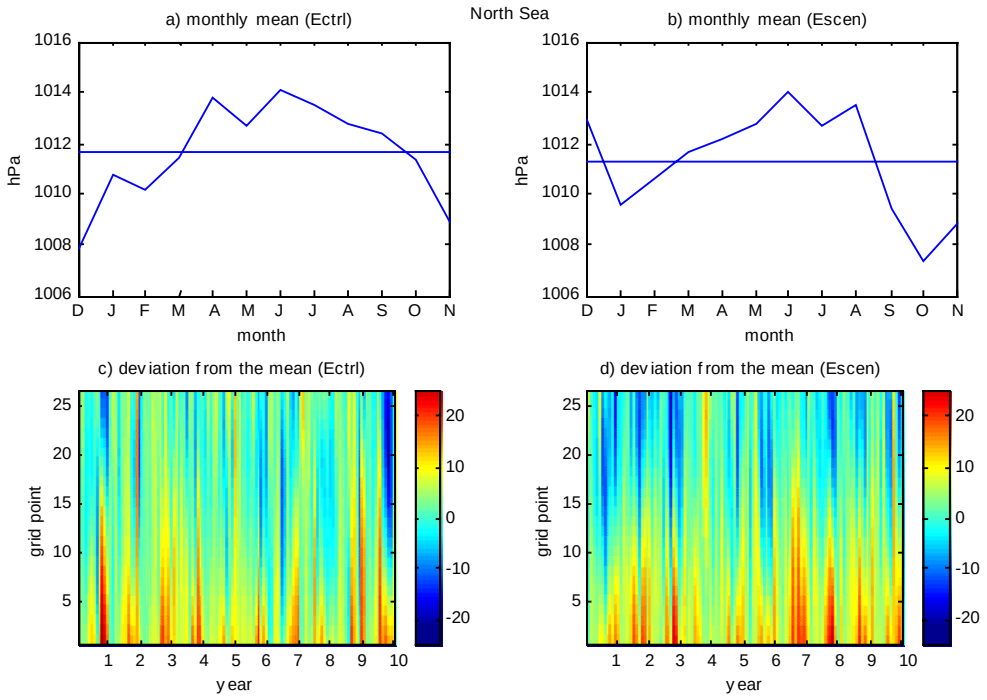

Figure 4.2 The top two graphs (a and b) shows the monthly mean sea level pressure for the North Sea profile for the ECHAM4 control and scenario run respectively. The dashed line shows the mean value. Under each respective graph is another graph (c and d) showing the deviation from the monthly mean sea level pressure for each month and grid point.

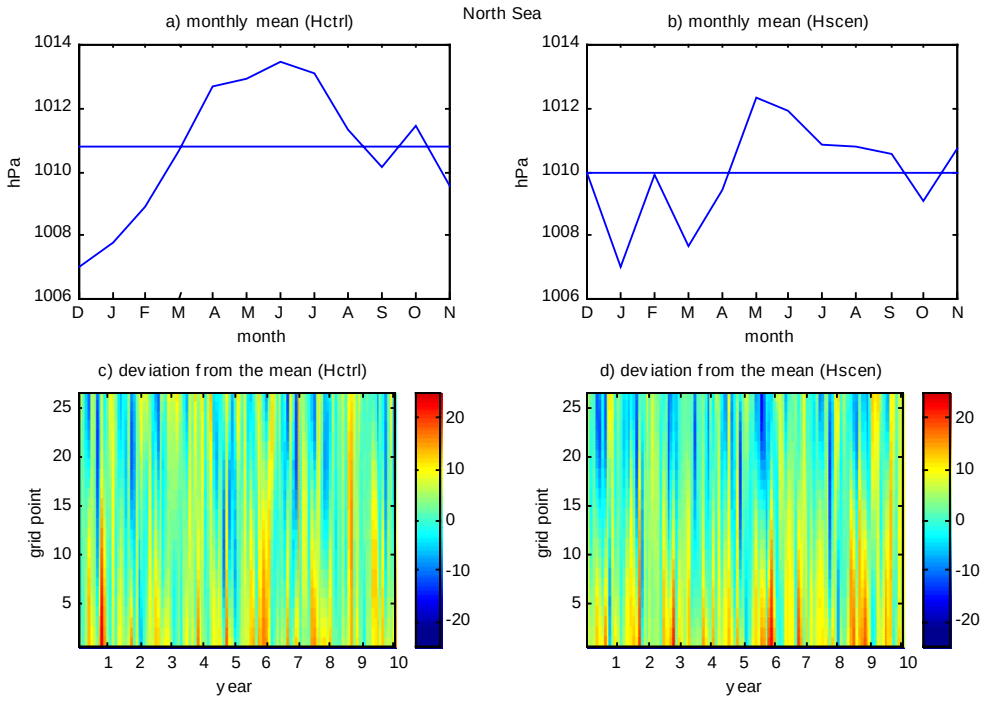

Figure 4.3 The top two graphs (a and b) shows the monthly mean sea level pressure for the North Sea profile for the HadCM2 control and scenario run respectively. The dashed line shows the mean value. Under each respective graph is another graph (c and d) showing the deviation from the monthly mean sea level pressure for each month and grid point.

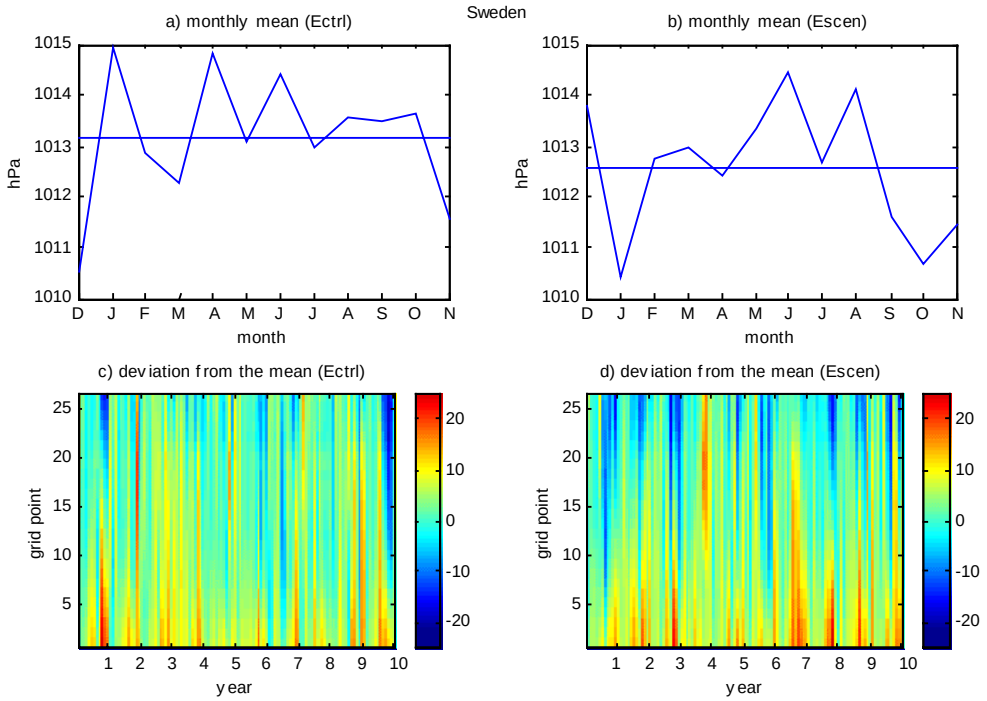

Figure 4.4 The top two graphs (a and b) shows the monthly mean sea level pressure for the Swedish profile for the ECHAM4 control and scenario run respectively. The dashed line shows the mean value. Under each respective graph is another graph (c and d) showing the deviation from the monthly mean sea level pressure for each month and grid point.

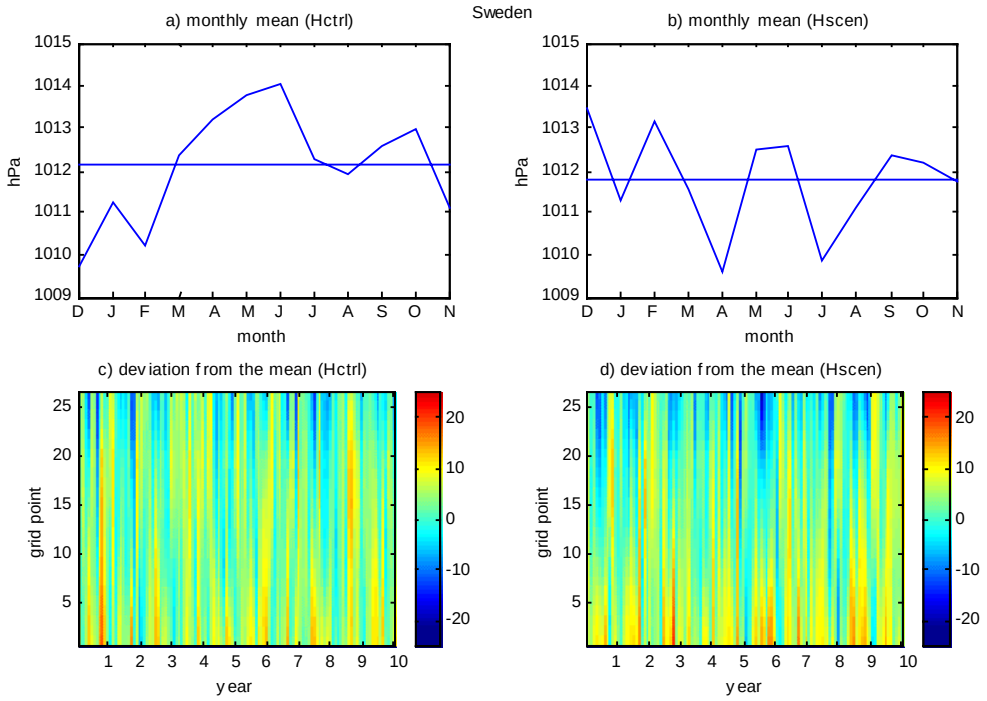

Figure 4.5 The top two graphs (a and b) shows the monthly mean sea level pressure for the Swedish profile for the HadCM2 control and scenario run respectively. The dashed line shows the mean value. Under each respective graph is another graph (c and d) showing the deviation from the monthly mean sea level pressure for each month and grid point.

4.1.3 Grid point frequency of lowest pressure

Decadal average

The grid point with the highest frequency of lowest pressure during the 10-year period is the northernmost grid point (26). An interesting feature in figure 4.6 is that the HadCM2 run for the Ns profile shows an increased frequency of lowest pressure in the scenario run in the northernmost grid points and a decrease in the southernmost grid points compared to the control run. This pattern is also present in the other Ns run as well as in both runs for the Sw profile (not shown).

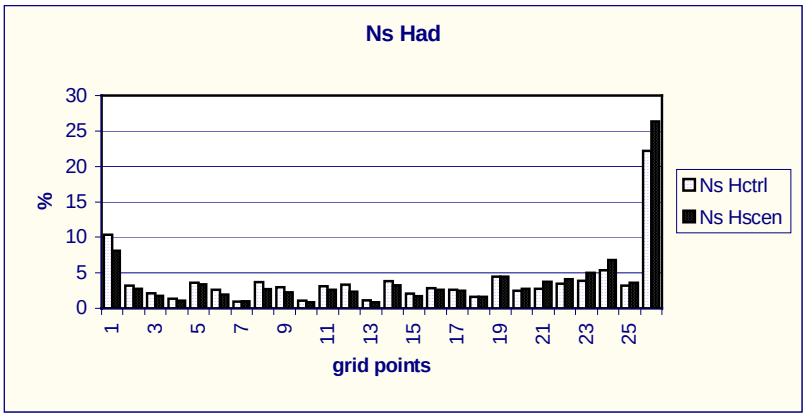

Figure 4.6 The grid point distribution of the frequency of lowest sea level pressure during a decade in the North Sea profile for the HadCM2 run. The left column shows the control run, the right the scenario run. The same pattern of distribution is also seen in all other runs for either profile.

Summer and winter mean

The distribution of the frequency of lowest pressure between the different grid points during summer and winter are not very different from the decadal averages. The grid point with the highest frequency of lowest pressure is still the northernmost grid point. The tendency towards an increase in the frequency of lowest pressure in the north and a decrease in the south in the scenario run compared to the control run is still there. The two exceptions are the frequency of lowest pressure during summer in the Sw profile for the ECHAM4 run and the frequency of lowest pressure during winter in the Ns profile for the HadCM2 run. These two graphs (figure 4.7 and 4.8) instead shows an increase in the scenario run compared to the control run in most grid points in the south as well as in the north.

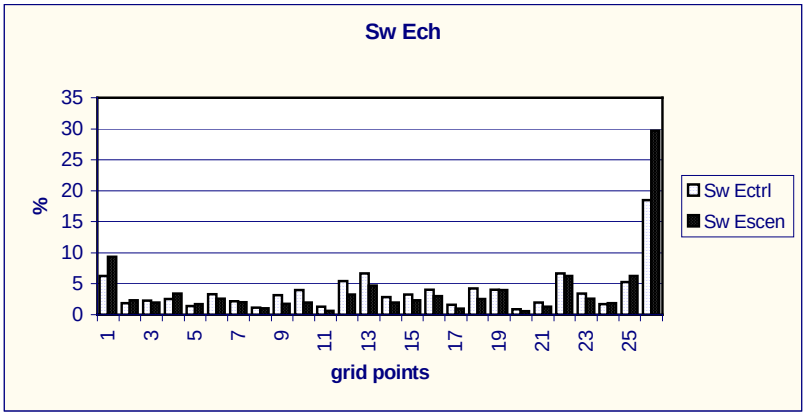

Figure 4.7 The grid point distribution of the frequency of lowest sea level pressure during summer in the Swedish profile for the ECHAM4 run. The left column shows the control run, the right the scenario run.

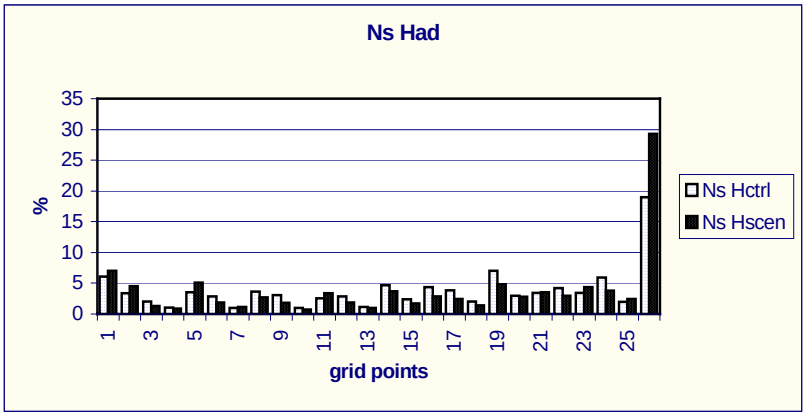

Figure 4.8 The grid point distribution of the frequency of lowest sea level pressure during winter in the North Sea profile for the HadCM2 run. The left column shows the control run, the right the scenario run.

4.1.4 Zonality

A common feature in the zonality, as can be seen in the box plots in figures 4.9 and 4.10, is that there is an increase in the zonality in the scenario run compared to the control run. Autumn is the season that shows the largest increase between the control and scenario runs, this increase varies between 4 and 7 hPa, the highest difference being when using ECHAM4 runs and the smallest when using HadCM2 runs. Also the increase is 1 hPa higher in the Ns than in Sw profile. The rest of the year the increase varies between 1 and 4 hPa, with the Ns profile showing the highest increase. The zonality shows the smallest standard deviations in summer. The largest standard deviations can be found in the winter season. Other than that the standard deviation does not show any noticeable differences, neither between the runs nor between the profiles.

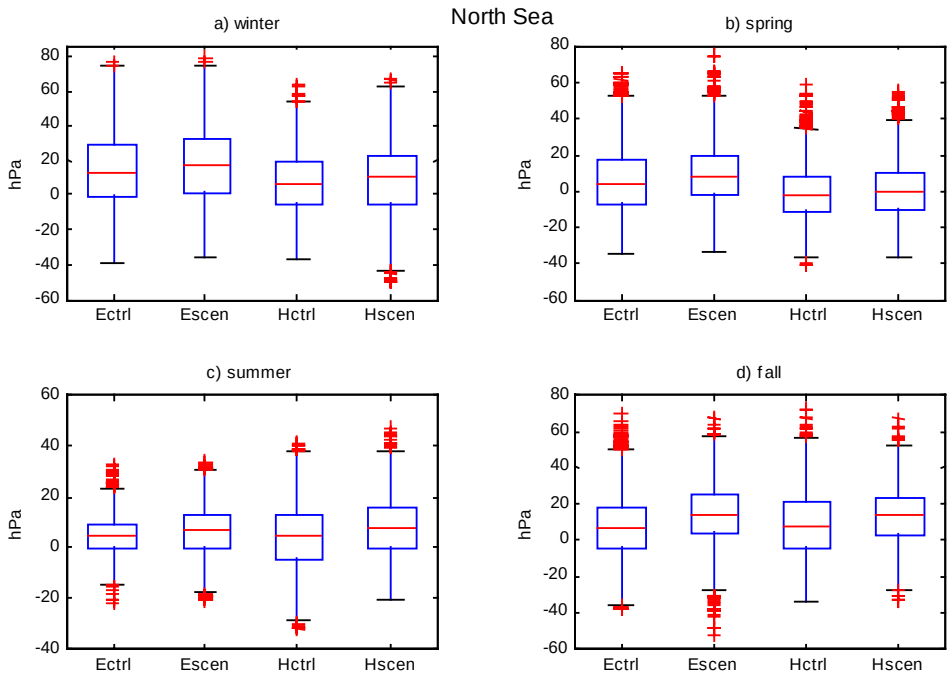

Figure 4.9 Box plots of the zonality for the 4 different seasons for the North Sea profile.

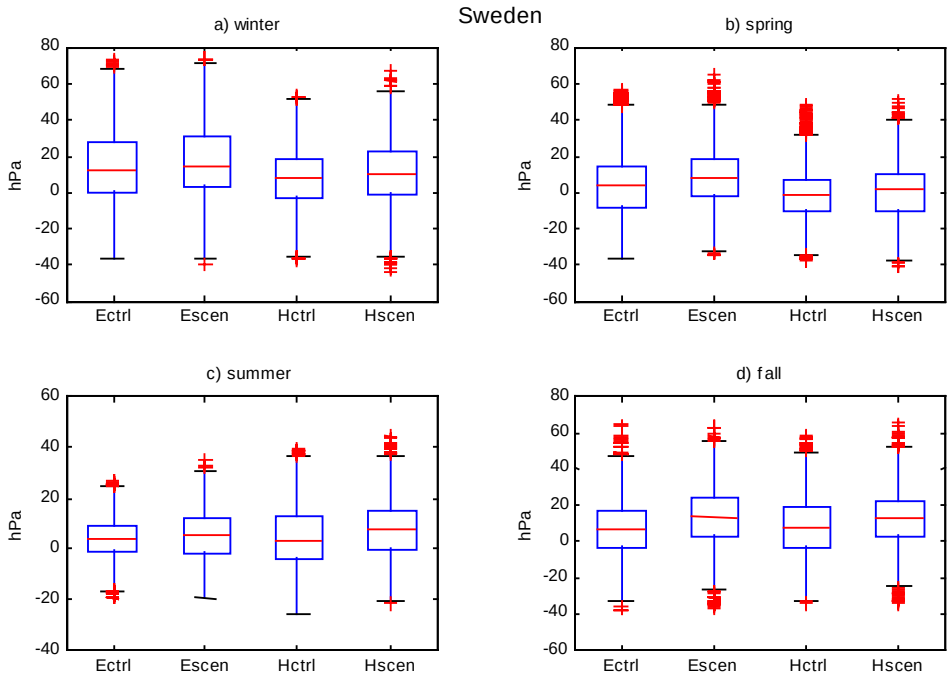

Figure 4.10 Box plots of the zonality for the 4 different seasons for the Swedish profile.

4.2 Geostrophic wind

4.2.1 Yearly mean

The yearly mean wind speed, as can be viewed in the box plots in figure 4.11, is higher in ECHAM4 than in HadCM2 in both profiles. The wind speeds are higher (in the order of 1 m/s) in the Ns profile than in the Sw profile. The scenario run in the Ns profile has slightly higher yearly mean values than the control run. In the Sw profile the ECHAM4 model shows a tendency towards a small (less than 0.5 m/s) reduction in wind speed whereas HadCM2 run shows a small (less than 0.5 m/s) increase in wind speed.

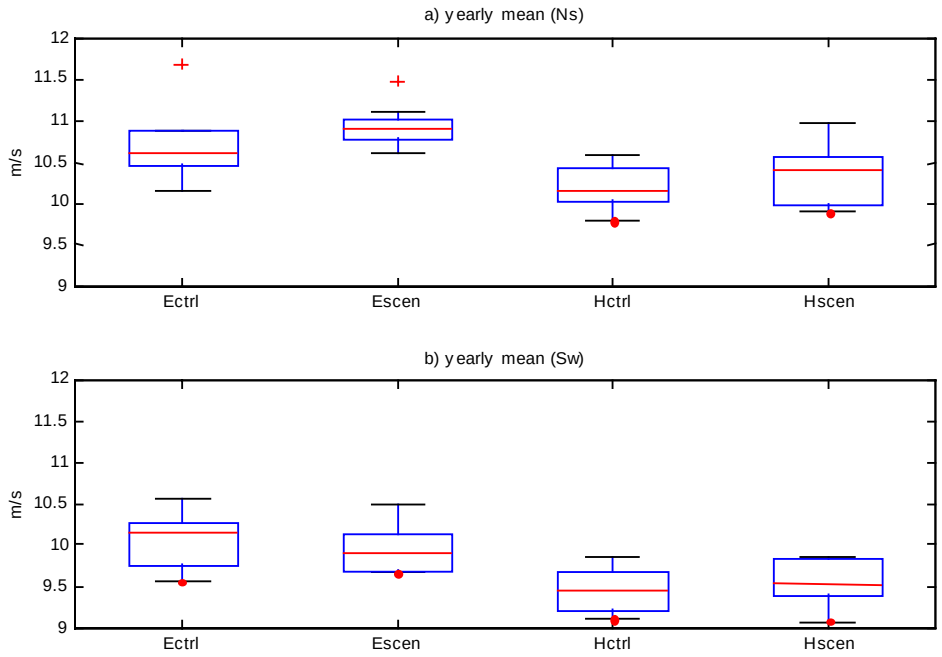

Figure 4.11 Yearly mean geostrophic wind speed for the North Sea (a) and the Swedish (b) profile.

A statistical test was conducted to see if there are any significant differences between the scenario and control runs. The Mann-Whitney test, a non-parametric test that requires equal variances, was chosen when all of the runs in figure 4.11 were found to have equal variances using the F-test. The resulting p-values from the test can be seen in table 4.3. Only the ECHAM4 run for the Ns profile was found to have a significant difference between the scenario and the control run at a 95% confidence interval.

Table 4.3 p-values from the Mann-Whitney test at alpha=0.05. Significant value in bold letters.

	P-values
ECHAM4 Ns	**0.038**
HadCM2 Ns	0.623
ECHAM4 Sw	0.427
HadCM2 Sw	0.791

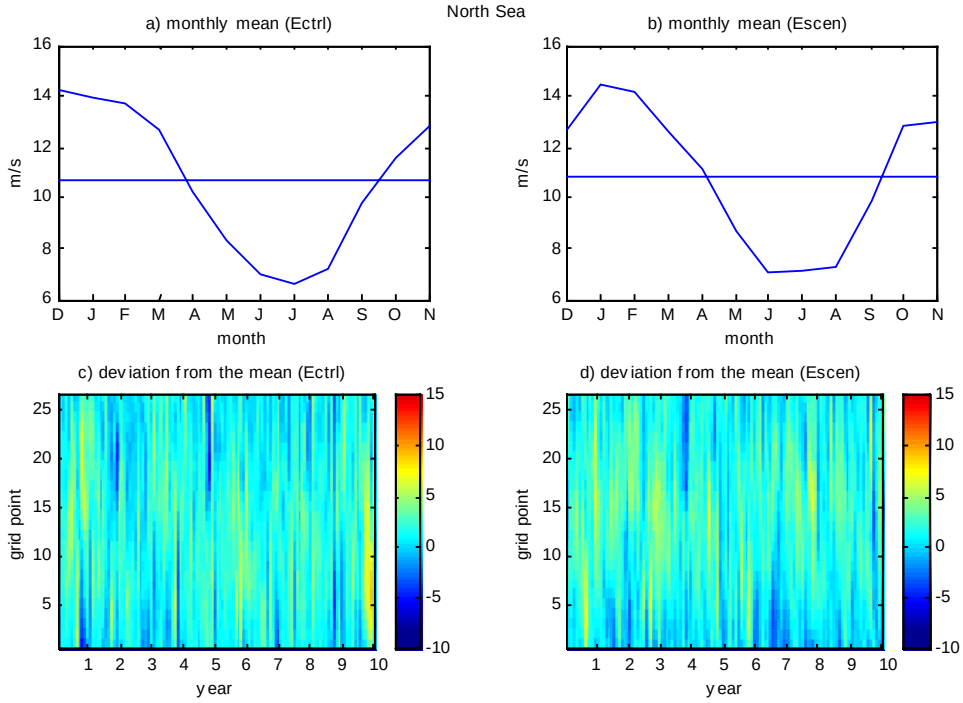

Figure 4.12 The top two graphs (a and b) shows the monthly mean geostrophic wind speed for the North Sea profile for the ECHAM4 control and scenario run respectively. The dashed line shows the mean value. Under each respective graph is another graph (c and d) showing the deviation from the monthly mean wind speed for each month and grid point.

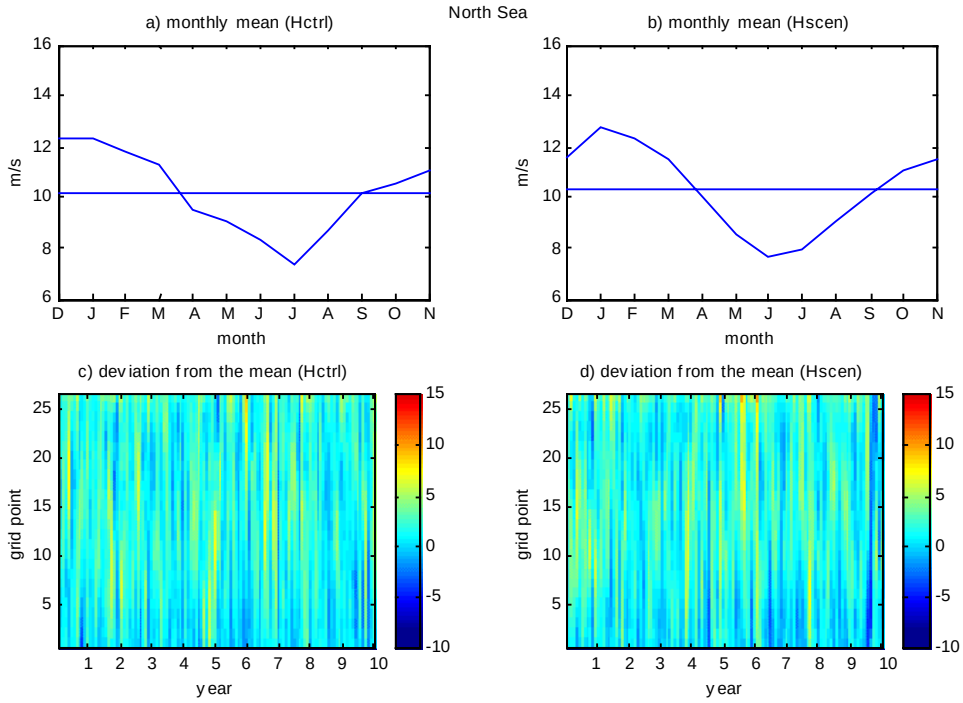

Figure 4.13 The top two graphs (a and b) shows the monthly mean geostrophic wind speed for the North Sea profile for the HadCM2 control and scenario run respectively. The dashed line shows the mean value. Under each respective graph is another graph (c and d) showing the deviation from the monthly mean wind speed for each month and grid point.

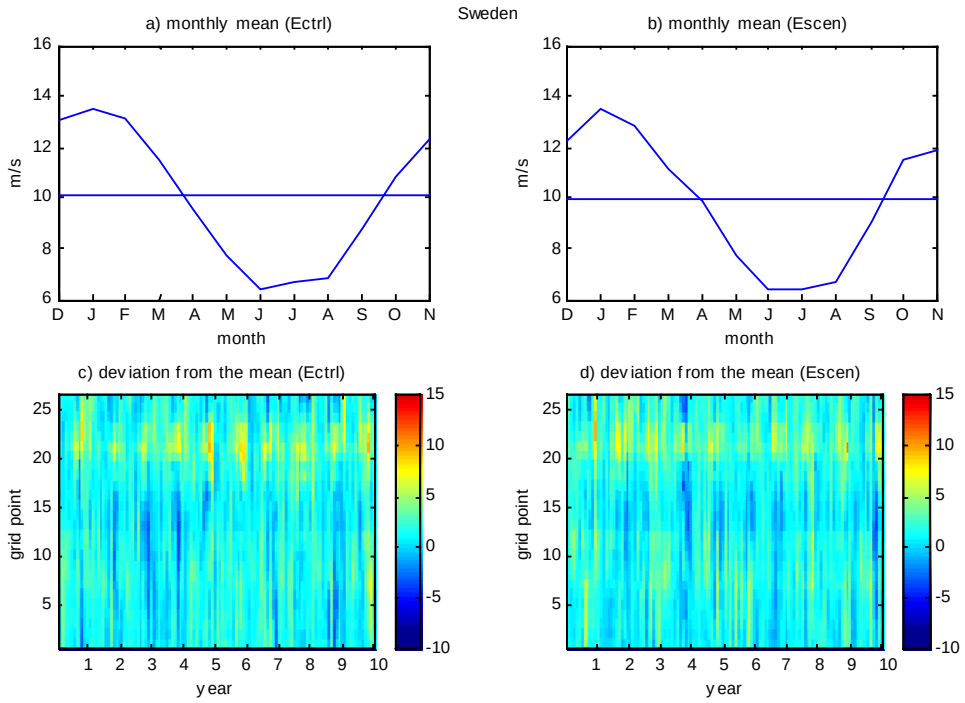

Figure 4.14 The top two graphs (a and b) shows the monthly mean geostrophic wind speed for the Swedish profile for the ECHAM4 control and scenario run respectively. The dashed line shows the mean value. Under each respective graph is another graph (c and d) showing the deviation from the monthly mean wind speed for each month and grid point.

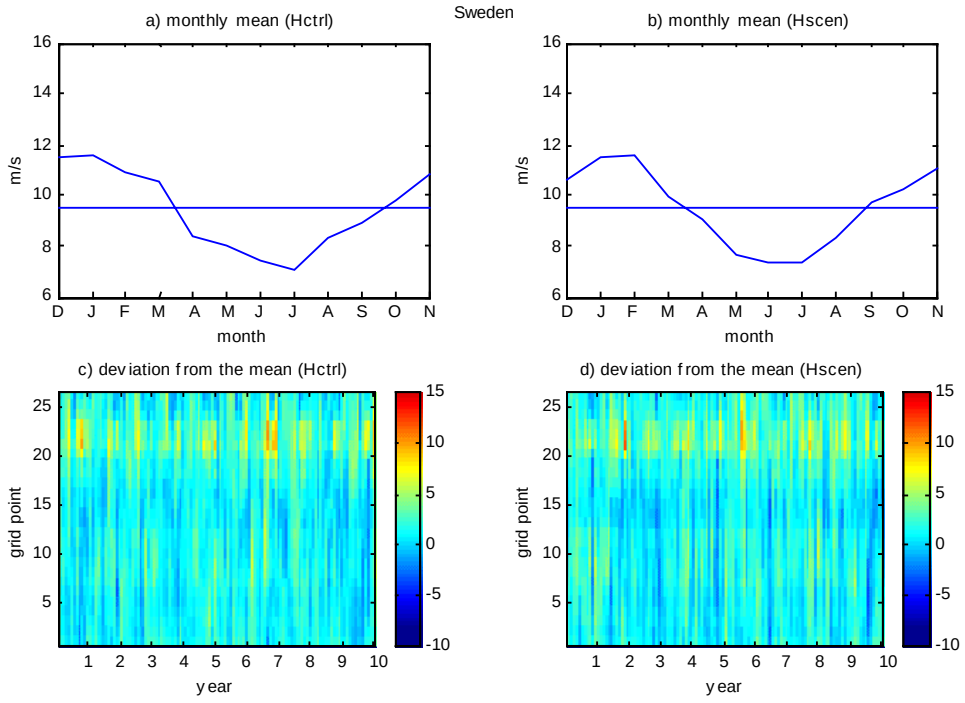

Figure 4.15 The top two graphs (a and b) shows the monthly mean wind speed for the Swedish profile for the HadCM2 control and scenario run respectively. The dashed line shows the mean value. Under each respective graph is another graph (c and d) showing the deviation from the monthly mean wind speed for each month and grid point.

4.2.2 Monthly mean

The seasonal variation, with highest wind speeds in winter (Dec – Feb) and autumn (Sep – Nov) and a minimum in wind speed during the summer (June – Aug), is very clear in figures 4.12 - 4.15 for both the Ns and Sw profile. The ECHAM4 run has slightly higher amplitude (about 1-2 m/s) compared to the HadCM2 run in both profiles. The scenario and the control are very similar and there doesn't appear to be any major changes between them, except for a trend toward a lower wind speed in December in the scenario. This trend can be found in both profiles. From figures 4.14 c) and d) and 4.15 c) and d) it is evident that the highest wind speeds in the Sw profile is experienced by the northernmost grid points (grid points 20-23) in winter. The Ns profile shows a more even distribution between north and south.

4.2.3 Change (scenario-control)

The yearly mean change in wind speed in figure 4.16 shows large intra decadal variability. There is a trend towards a very small increase in wind speed in both models for the Ns profile but a decrease for the Sw profile when running the model with ECHAM4 boundary data. The HadCM2 run for the Sw profile shows a small increase in wind speed due to the greenhouse effect (less than 0.2 m/s), but with a large variability. From the seasonal variation in figure 4.17 there is a trend towards a reduction in wind speed (0.7 – 1.5 m/s) during December. The Ns profile shows a small increase in wind speed (~0.5 m/s) the rest of the year, except for a decrease in May and June with HadCM2. The Sw profile shows no clear trend toward either a decrease or an increase in wind speed during the remaining months of spring or during summer. Early autumn shows a modest increase in wind speed (~0.5 m/s).

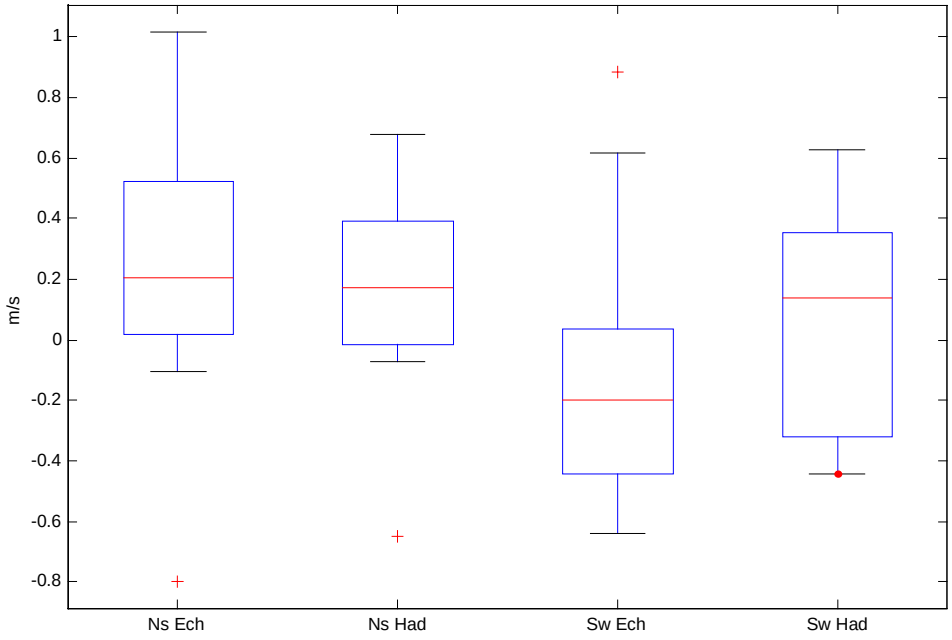

Figure 4.16 Yearly mean climate change (scenario – control) of the geostrophic wind speed.

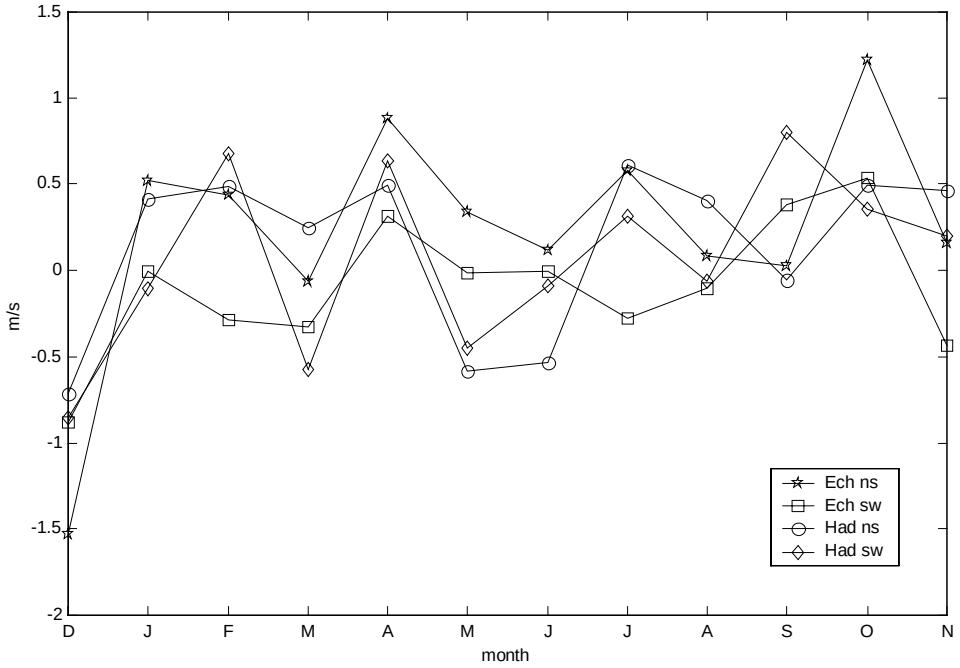

Figure 4.17 Monthly mean climate change (scenario – control) of the geostrophic wind speed.

4.2.4 Wind direction

The wind direction for 3 locations (north, middle and south) in the North Sea profile can be seen in the wind roses in figures 4.18 and 4.19. There is a clear distinction between the wind direction in the north and south in all runs. In the south the dominating wind directions are from the west and southwest. In the north and also in the middle of the profile the dominating wind direction is from the south and southwest. A common feature in these wind roses is the increase in the frequency of southwesterly and westerly wind directions in the scenario run (the three wind roses at the bottom of each figure). This increase is accompanied with a decrease of the frequency of north, northeast, east and southeast wind directions in the north and middle of the profile as well as in the south in the HadCM2 run. In the south (the rightmost wind roses) in the ECHAM4 run there is little change in the frequency of wind directions from the north, northeast, east and southeast.

The frequency of different wind directions for 3 locations (north, middle and south) in the Sw profile can be seen in figures 4.20 and 4.21. The northern part of the Sw profile are dominated by a wind from the south, the middle is dominated by wind from the southeast and also from the southwest except for the HadCM2 control run. In the southern most past of the Sw profile, the winds come mainly from the west and in the HadCM2 run also from the southeast. In all wind roses for the scenario runs in the Sw profile there is an increase in the frequency of northwesterly and westerly winds. The south, southeast and easterly wind direction shows a decrease in the scenario run compared to the control run.

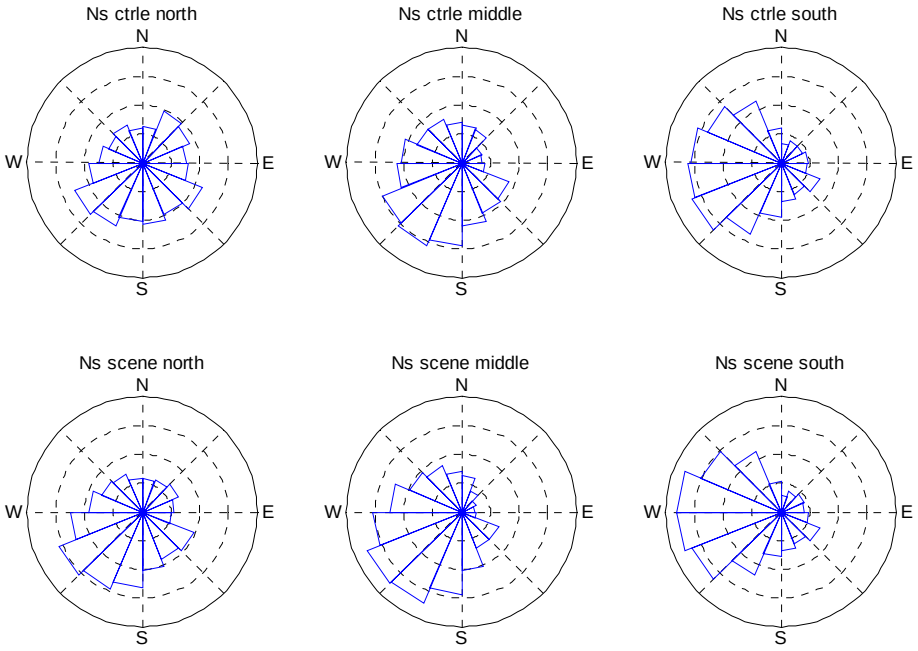

Figure 4.18 Wind direction in the north, middle and south (mean of grid points 19-21, 12-14 and 6-8 respectively) of the North Sea profile for the ECHAM4 run. Each of the dashed rings in the wind rose represents a frequency of 500 values. The top three wind roses are from the control run, underneath each of these are their respective scenario run.

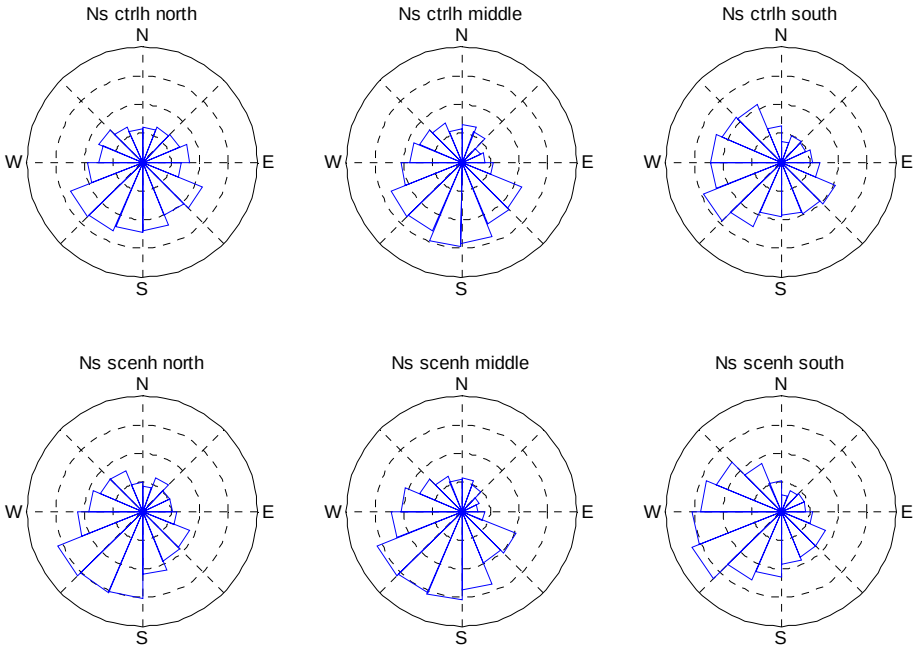

Figure 4.19 Wind direction in the north, middle and south (mean of grid points 19-21, 12-14 and 6-8 respectively) of the North Sea profile for the HadCM2 run. Each of the dashed rings in the wind rose represents a frequency of 500 values. The top three wind roses are from the control run, underneath each of these are their respective scenario run.

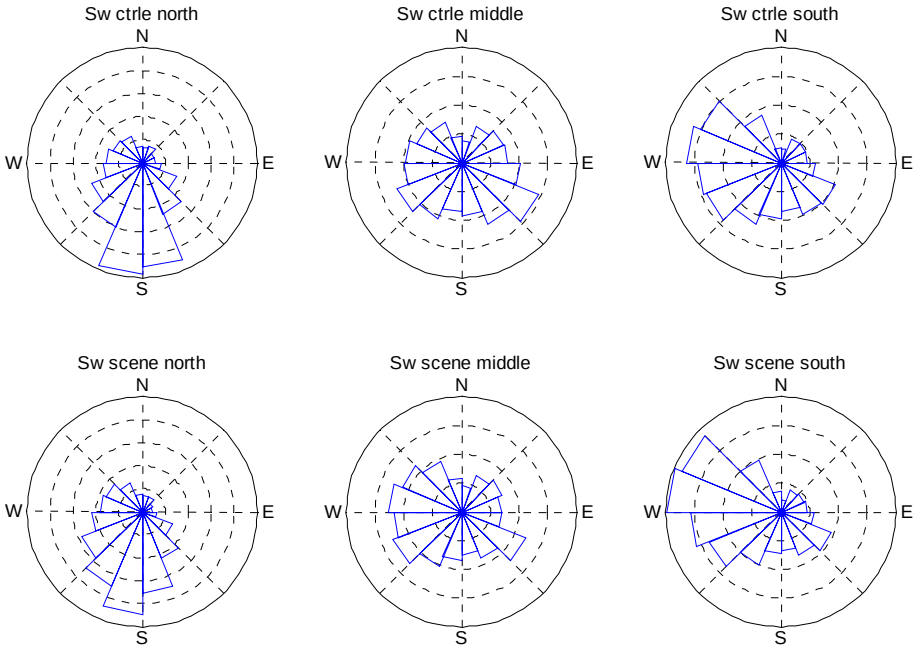

Figure 4.20 Wind direction in the north, middle and south (mean of grid points 20-22, 13-15 and 7-9 respectively) of the Swedish profile for the ECHAM4 run. Each of the dashed rings in the wind rose represents a frequency of 500 values. The top three wind roses are from the control run, underneath each of these are their respective scenario run.

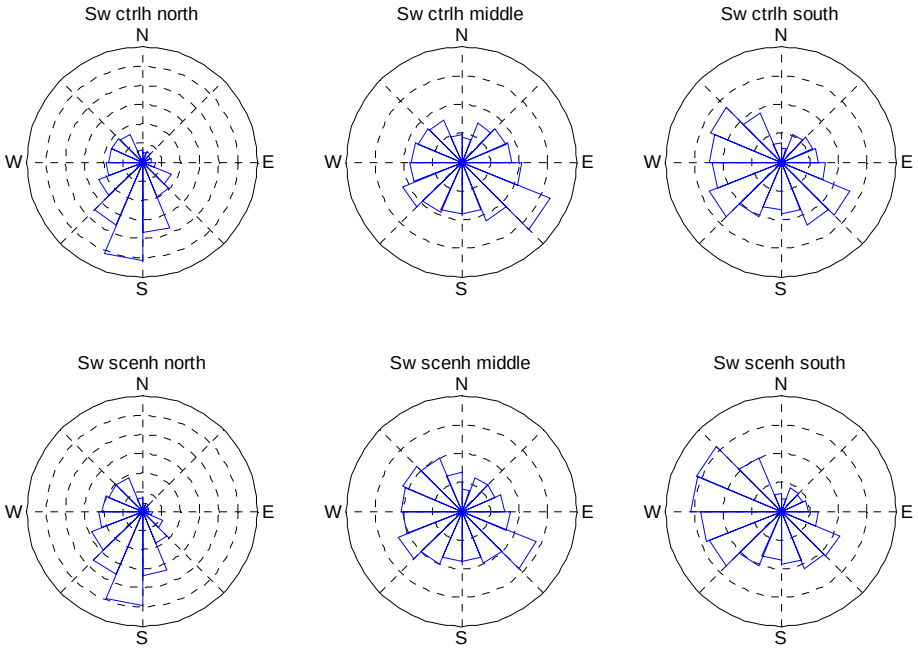

Figure 4.21 Wind direction in the north, middle and south (mean of grid points 20-22, 13-15 and 7-9 respectively) of the Swedish profile for the HadCM2 run. Each of the dashed rings in the wind rose represents a frequency of 500 values. The top three wind roses are from the control run, underneath each of these are their respective scenario run.

4.2.5 Percentiles

The yearly mean of the percentiles can be seen in figure 4.22. There is a clear difference between the ECHAM4 and HadCM2 runs. ECHAM4 clearly has larger values than HadCM2, in the order of 2-3 m/s. The Ns profile shows a tendency towards higher yearly mean percentiles in scenario compared to control, especially when looking at the 95 percentiles. In the Sw profile there is no noticeable increase in the percentiles between control and scenario in the HadCM2 run. In the ECHAM4 run for the Sw profile there is a decrease in percentile values between control and scenario. The monthly variation of the 95 and 99 percentiles can be found in figure 4.23. ECHAM4 clearly has larger seasonal amplitude than HadCM2. ECHAM4 shows higher percentiles (both 95 and 99) in winter than HadCM2, but smaller percentiles in summer. The differences between control and scenario are small in all four graphs.

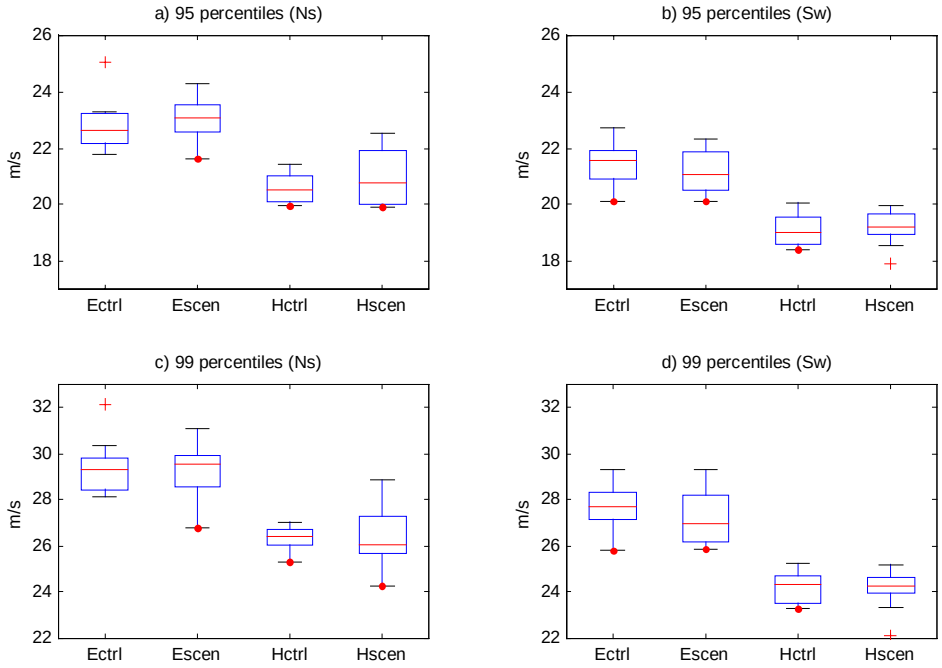

Figure 4.22 Box plots of the yearly variation of the geostrophic wind percentiles. The top two graphs (a and b) show the 95 percentiles and the bottom two (c and d) the 99 percentiles. To the left (a and c) are the percentiles for the North Sea profile and to the right (b and d) for the Swedish profile.

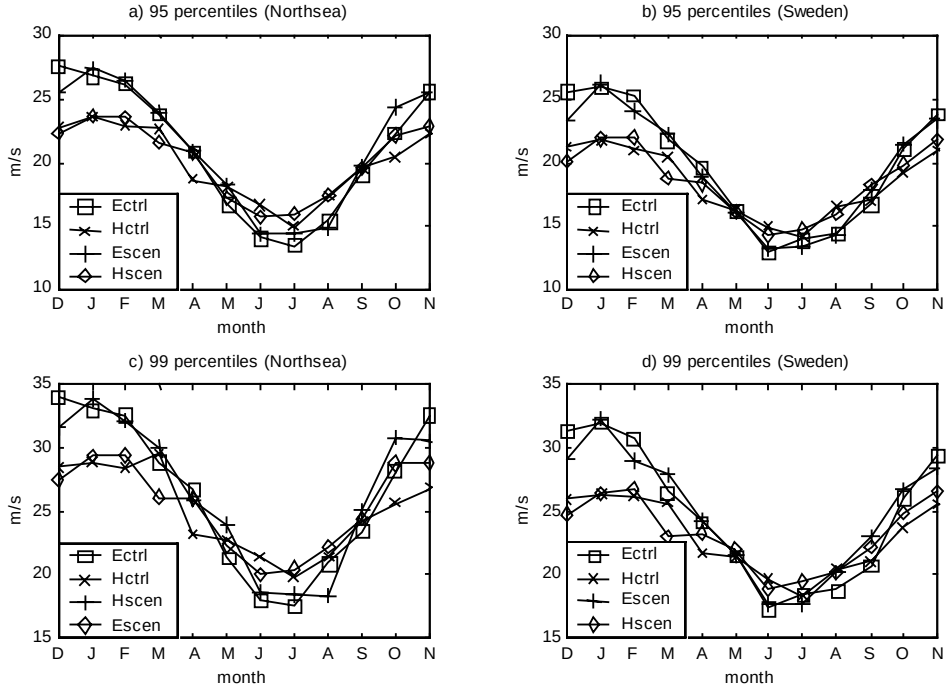

Figure 4.23 The monthly variation of the 95 (top two graphs) and 99 (the two graphs on the bottom) percentiles of the geostrophic wind. To the left (a and c) are the percentiles for the North Sea profile and to the right (b and d) for the Swedish profile.

4.2.6 Seasonal variation in the intensity of strong winds and storms

Figures 4.24 – 4.27 shows the seasonal variation of the highest wind intensities, in the form of percentages of wind speeds exceeding 20 or 25 m/s. Winter is clearly the dominating season for strong winds and storms, followed by autumn and spring. The difference between the ECHAM4 and HadCM2 runs is largest during winter followed by autumn. This difference with larger seasonal amplitude in the ECHAM4 run was also observed in the monthly analyses of the 95 and 99 percentiles in figure 4.23. There is an increase in figures 4.24 and 4.26 between the control and scenario runs during autumn in the Ns profile. Though the difference is larger in figure 4.24, which shows the percentage of winds over 20 m/s. Winter shows a small decrease in wind intensity, but only when using the ECHAM4 run. The other seasons for the North Sea profile shows little change between scenario and control runs. The Sw profile shows an increase between control and scenario during autumn, but only in the HadCM2 run in figure 4.25 (percentage of winds over 20 m/s). The ECHAM4 run shows a decrease in the percentage of winds over 20 and 25 m/s during winter in the Sw profile.

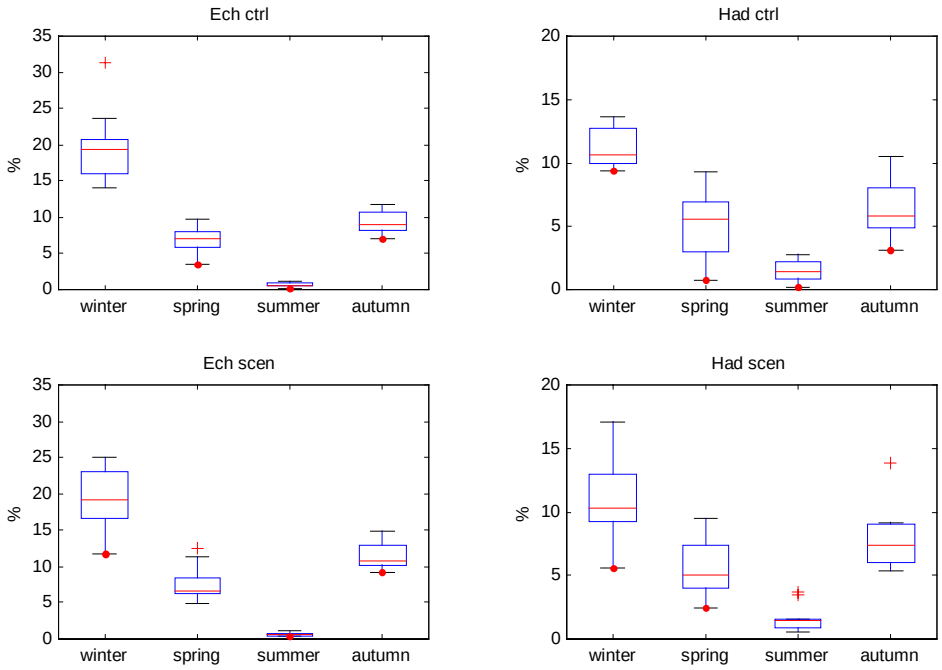

Figure 4.24 Percentage of geostrophic winds over 20 m/s in winter, spring, summer and autumn for the North Sea profile.

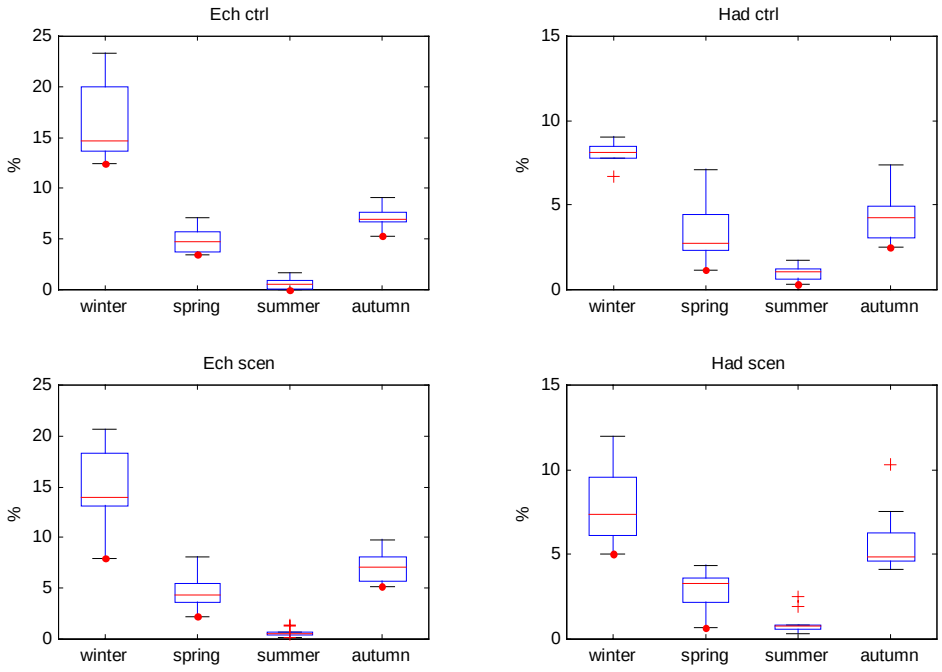

Figure 4.25 Percentage of geostrophic winds over 20 m/s in winter, spring, summer and autumn for the Swedish profile.

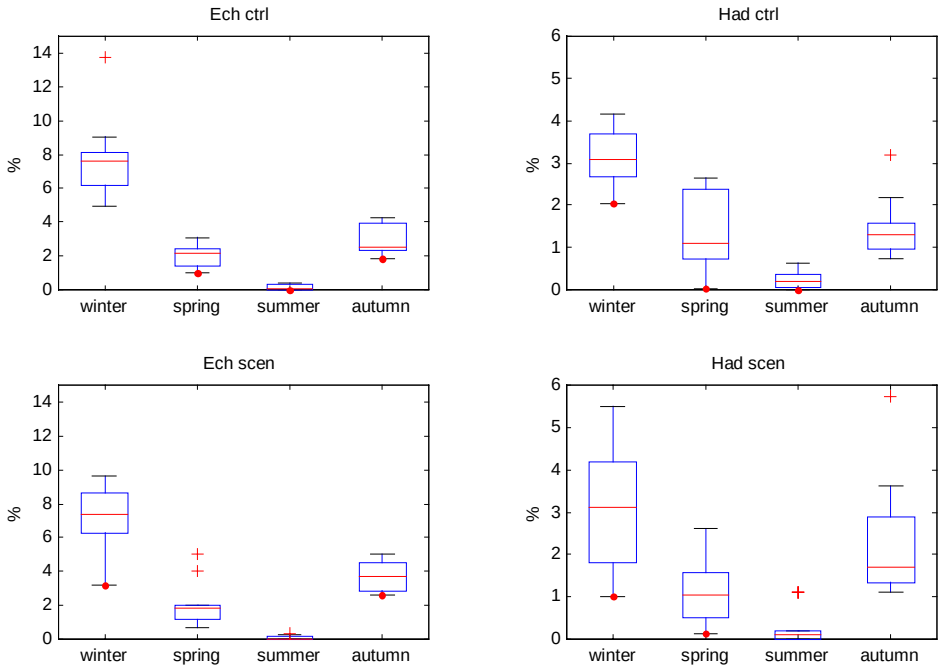

Figure 4.26 Percentage of geostrophic winds over 25 m/s in winter, spring, summer and autumn for the North Sea profile.

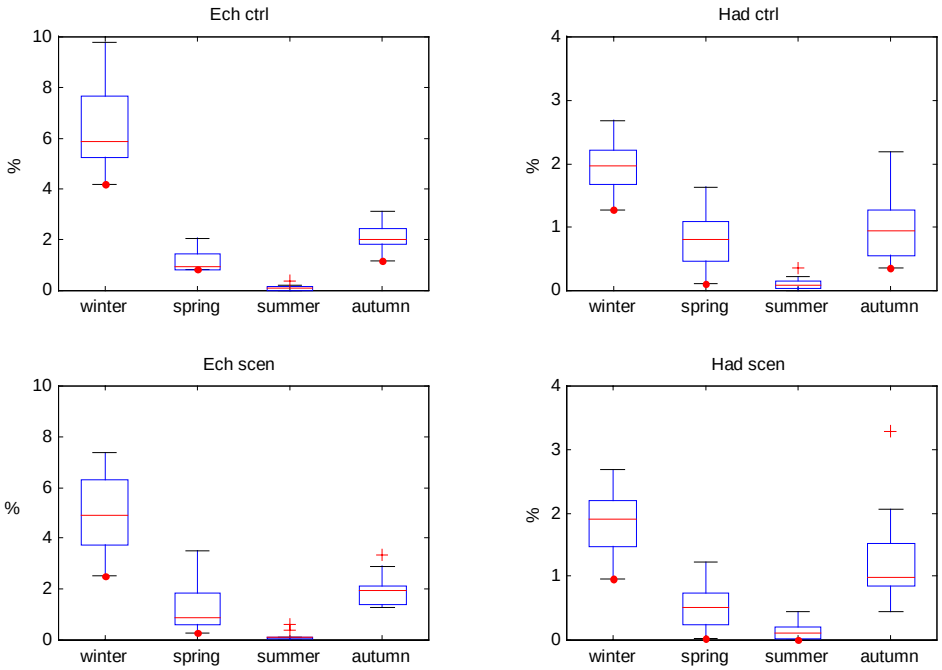

Figure 4.27 Percentage of geostrophic winds over 25 m/s in winter, spring, summer and autumn for the Swedish profile.

4.3 Statistics

4.3.1 Variance analysis

The results from the balanced ANOVA analysis on the monthly values of the sea level pressure and the geostrophic wind can be seen in table 4.4. The table only shows the result of the following 3 variables: Model (HadCM2 or ECHAM4), Area (North Sea or Sweden) and Run (control or scenario). Other combinations were also calculated (Model*Area, Model*Run, Area*Run, Model*Area*Run) but no statistically significant differences could be found. The p-values for the geostrophic wind (right hand columns of table 4.4) shows clearly that the variables with a statistically significant variance at a 95 % confidence interval, are the Model and the Area. These result points at a significant difference between the two models used for boundary data as well as between the two profiles, but no significant difference between the Runs.

Table 4.4 p-values from the ANOVA analysis. Significant values are in bold letters.

	Sea level pressure			Geostrophic wind		
variables	north	middle	south	north	middle	south
Model	0.990	0.133	**0.000**	**0.028**	**0.001**	**0.000**
Area	**0.000**	**0.000**	0.486	**0.000**	**0.000**	**0.000**
Run	**0.000**	0.113	0.057	0.326	0.679	0.640

The p-values for the sea level pressure (table 4.4) on the other hand show a very high correspondence between the Models in the northern part of the profile, whereas in the south there is absolutely no correlation between the Models. The two Areas show a significant difference in the northern and middle part of the profile, but no significant difference can be found in the south. The only location with a statistically significant difference between the Runs is in the north. In the middle and south there are no significant difference between the Runs, but the low values suggests there being a larger difference than between the Runs at the same locations in the geostrophic wind analysis.

5 Discussion

5.1 The atmospheric pressure distribution

The simulated monthly mean sea level pressure is higher in summer than in winter, which corresponds well with the real pressure situation in Europe. Also the pressure difference between north and south (the zonality) being largest in winter indicates the domination of the Icelandic low-pressure system in that season. The monthly mean sea level pressure shows very little seasonal variation over Swedish and northern Germany compared to over the North Sea and the Norwegian Sea. A reason for this is the influence of the Scandinavian Mountains and local/regional scale effects of the land surface heterogeneity.

The two scenario runs (using HadCM2 and ECHAM4 boundary data respectively) are well in agreement about the effect of an increased CO_2 concentration on the atmospheric pressure distribution. Both the increased frequencies of low-pressure “passages” in the northern parts

of both profiles, along with an increased zonality suggest a deepening of the Icelandic low-pressure centre. An increased meridional pressure gradient has also been found in other studies of the effects of climatic change, for example by Carnell et al (1996). The increase in the frequencies of northerly low-pressure centres is very likely related to the downstream intensification of the Atlantic storm track due to en enhanced greenhouse effect as found by for example Beersma et al (1997) & Lunkeit et al (1998).

5.2 Regional changes in the wind circulation

The seasonal variation of the geostrophic wind speed shows very little variation within the North Sea profile. The northernmost grid points in the Swedish profile have slightly higher wind speeds in winter than compared to the rest of the profile. This is most likely an effect of these being coast grid cells. The seasonal variation with lowest wind speed during summer and higher wind speed during winter and autumn is well in agreement with the real wind situation over Europe. Autumn and winter are the seasons that bring us the highest frequencies of storms, which naturally give these seasons a higher monthly mean wind speed. There is clearly a significant difference between the monthly mean geostrophic wind values of the North Sea profile and the Swedish profile.

There is an overall trend towards a reduction of the wind speed during winter and a modest increase of the wind speed during autumn in both profiles. But these are not statistically significant.

The yearly mean values only showed significant change between the control and scenario runs in the North Sea profile when modelled using ECHAM4 boundary data. This change is in the form of an increase in the annual mean geostrophic wind speed of 0.2 m/s. When using HadCM2 boundary data there is also an increase in the North Sea profile due to climatic change. This increase is of about the same magnitude (0.2 m/s) as when using the other model, but the increase is not statistically significant. The increase in wind speed in the North Sea profile is most noticeable during autumn (especially in October), showing an increase of around 0.5-1.0 m/s. The higher value being when using ECHAM4 boundary data. This increase is likely to be a consequence of the increase in the meridional pressure gradient, which is mostly expressed in autumn.

The Swedish profile also shows a small but statistically non-significant increase in yearly mean wind speed when using HadCM2 boundary data. The statistically non-significant decrease in yearly mean wind speed in the Swedish profile as seen when using ECHAM4 boundary data, is most likely because the large decrease in December (1.5 m/s) totally offsets the increase in wind speed (up to 0.5 m/s) during the rest of the year. That the increase in wind speed is smaller in the Swedish than the North Sea profile can be explained by the fact that the meridional pressure gradient increase is smaller over The Swedish profile.

Winds from the west and southwest are common in southern Scandinavia throughout most of the year. This compares well with my analyses of the wind directions. The model shows an increased frequency of westerly winds due to the enhanced greenhouse effect, this will mean that northwestern Europe (mainly England, Denmark, Sweden and Norway) will experience an increased maritime climate. Combined with a low frequency of northern winds this will bring less severe winters. The increased frequency of northwesterly and westerly winds combined with a decrease in the south, southeast and easterly winds over Sweden will,

according to Jönsson & Fortuniak (1995), bring lower annual temperatures. Because of the increased maritime influence on the climate this implies cooler summers ahead as a consequence of a doubled concentration of CO_2 in the atmosphere.

5.3 Changes in the intensity of strong winds

In the North Sea profile there is a tendency towards an increase in the intensity of gale winds and also of storm winds on a yearly mean basis. This increase is mostly expressed during autumn. In the run using ECHAM4 boundary data a trend towards a reduction in wind intensity can be found in winter. When using the other model as boundary data no change could be detected during winter. Contrary to my results the WASA Group (1998) found a weak increase in storm activity during winter in the North Sea, when studying 10% exceedence values of 10-m surface winds from a high-resolution climate change scenario. The North Sea constitutes most of the southern part of my North Sea profile. Though they found a decrease in the area covered by the northern part of my North Sea profile. I have not done any studies on the distribution over the profiles of the change in wind speed though, since the deviation from the monthly mean wind values showed little variation over the profile. Several studies, among them Ulbrich & Christoph (1999) & Beersma et al (1997) has found an increase in storm track activity over Europe during winter. This correlates well with the deepening of the Icelandic low-pressure centre in this area as I have found in my analysis. Ulbrich & Christoph (1999) found a positive correlation between the intensification of the 500 hPa storm track over northern Europe and higher NAO values. Thus an increase in storm track strength can be related to an increase in the meridional pressure gradient. An increased pressure gradient leads to stronger winds thus causing an increase in the air – sea fluxes, which enforce the baroclinicity. The increased growth of baroclinic waves due to the enforced baroclinicity means larger storm track activity. The relationship between the storm track activity and the pressure gradient can also explain why I found the increase in storm intensity during autumn since this season is the time of year that shows the highest increase in zonality due to the increased greenhouse warming.

A small increase in the intensity of gale winds in early autumn was found in the Swedish profile when using HadCM2 boundary data. But I found no increase in the intensity of storm winds over Sweden due to an enhanced greenhouse effect. When running the model with ECHAM4 boundary data, there is instead a decrease in the winter intensity of storm and gale winds over Sweden. A decrease in wind intensity over Sweden is in agreement with the results of the WASA Group (1998) who also found a decrease over most of Sweden due to the greenhouse effect when looking at the 10% exceedence values of 10 m wind speeds. South of Sweden and the Baltic Sea though, they found an increase in wind intensity.

5.4 Human and environmental impacts

Even a modest increase in the intensity of storm winds as found over the North Sea and the Norwegian Sea could have an impact on human activities and also on the environment. Most impacts from strong winds and storms are secondary. For example people that spend a lot of time at sea like for example fishermen or in offshore industries, are deeply influenced by the large waves generated by storms. These waves also cause damage on beaches and coastal areas when they encounter land. Storms also cause a lot of damage on houses and business, a rise in storm and/or gale intensity will lead to a large increase in storm damage (Dorland et al,

1999). Though a lot of this increased damage is due to population and economic growth, increased storm intensity is naturally an important factor that can substantially increase the economic losses after a storm.

The environment is also influenced by changes in the wind strength. Of specific interest to humans is the damage to forest. The forest industry loses a lot of money when storms fell trees in planted forests. Franzen et al (1991) found a connection between the increased frequency of gales and the increased damage to coniferous forests on the Swedish West Coast. Spruce is very sensitive to salt deposition and western gales bring with them marine aerosols, which are deposited on the vegetation. The increased frequency of gales over the coastal continental areas as found when using HadCM2 boundary data, combined with increased westerly wind flow, and would worsen the conditions for the coniferous forests in the future.

5.5 How good/ reliable are the results

The goal when creating and running a climate model is naturally to achieve a climate that is as realistic as possible. Theoretically it is not possible to take into account every process that occur in nature and it is therefore important to remember that no matter how complex a model is, it is still only a simplified view of the real climate system (Trenberth, 1997). The reliability of the regional climate scenario in SWECLIM very much depends on the GCM used for boundary conditions. Any uncertainties in the GCM are inherited into the regional model.

In all calculations that were made, a large difference was easily detected when comparing the models using HadCM2 and ECHAM4 boundary data. This difference was most of the time larger than between the control and scenario runs. This was clearly demonstrated with the ANOVA-test, whose result can be seen in table 4.1. Only when comparing the pressure as modelled in the northern part of the two profiles could a high correlation be found between the two models. This is clearly a sign saying that there is still a lot of work needing to be done to improve the results of climate models.

To achieve a higher reliability in the results a higher resolution than the 88 km used here would be desirable along with a longer time series than 10 years. According to Rummukainen et al (1998) a 20 km resolution is desirable for regional impact studies. It also would have been interesting to make a comparison between the model data analysed and the real observed data, to get a picture of how realistic the results of this analysis really is.

6 Summary

- I found a change in the large-scale atmospheric pressure circulation due to an enhanced greenhouse effect. This change takes the form of an increased meridional pressure gradient, which suggests a deepening of the Icelandic low-pressure centre.
- There is a significant increase in the yearly mean geostrophic wind speed due to the climatic change in the North Sea and the Norwegian Sea when using ECHAM4 boundary data. This increase is in the magnitude of 0.2 m/s. The change when using HadCM2 boundary data is of the same magnitude but is not a statistically significant increase. The increase in geostrophic wind speed is linked to the increase in the meridional pressure gradient.

- The yearly mean geostrophic wind speed over Sweden and northern Germany shows a small (less than 0.2 m/s) increase in wind speed between the control and scenario runs when running the model with boundary data from the HadCM2 model. When using ECHAM4 for boundary conditions the yearly mean geostrophic wind shows a decrease of about –0.2 m/s due to the climatic change. None of these changes are statistically significant.
- There is a trend, though not a statistically significant one, towards a decrease of the wind speed in December and an increase in autumn of the mean geostrophic wind speed over northwestern Europe due to the greenhouse effect.
- The model shows an increase in the frequency of westerly winds. This means that northwestern Europe can come to experience an increased maritime influence on the climate as a result of a global warming.
- The model shows a future increase of the yearly mean intensity of storms and also of gale winds over the North Sea and the Norwegian Sea. This increase is mostly expressed in autumn. In winter there is a decrease in the intensity of strong winds when using ECHAM4 boundary data. I also found an increase in the intensity of gale winds on a yearly mean basis over Sweden when using the HadCM2 model as boundary data. When using ECHAM4 boundary data, the model showed a decrease in the winter intensity of storm and gale winds over Sweden.

7 References

Alexandersson, H.; Schmith, T.; Iden, K.; Tuomenvirta, H., 1998: Long-term variations of the storm climate over NW Europe. *Global Atm Ocean System,* 6: 97-120

Alexandersson, H.; Tuomenvirta, H; Schmith, T.; Iden, K., 2000: Trends of storms in NW Europe derived from an updated pressure data set. *Climate Research*, 14: 71-73.

Bacon, S., Carter D.J.T., 1991: Wave climate changes in the north Atlantic and North Sea. *Int. J. Climatol.*, 11: 545-558.

Bacon, S., Carter D.J.T., 1993: A connection between mean wave height and atmospheric pressure gradient in the north Atlantic. *Int. J. Climatol.*, 13: 423-436.

Beersma J., Rider K., Komen G., Kaas, E., Kharin, V., 1997: An analysis of extra-tropical storms in the North Atlantic region as simulated in a control and a 2 x CO2 time slice experiment with a high-resolution atmospheric model. *Tellus*, 49A**:** 347-361.

Carnell, R.E., Senior, C.A., 1998: Changes in mid-latitude variability due to increasing greenhouse gases and sulphate aerosols. *Clim. Dyn.*, 14: 369-383.

Carnell, R.E., Senior, C.A., Mitchell, J.F.B., 1996: An assessment of measures of storminess: simulated changes in Northern Hemisphere winter due to increasing CO_2. *Clim. Dyn.*, 12: 467-476.

Chen, C.T., Roeckner, E., 1996: Cloud simulations with the Max-Planck-Institute for meteorology general circulation model ECHAM4 and comparison with observations. *Max-Planck-Institute for Meteorology, Report No. 193*, Hamburg, Germany, 49 pp.

Corti, S., Molteni, F., Palmer, T.N., 1999: Signature of recent climate change in frequencies of natural atmospheric circulation regimes. *Nature,* 398: 799-802.

Dorland, C., Tol, R.S.J., Palutikof, J.P., 1999: Vulnerability of the Netherlands and northwestern Europe to storm damage under climate change. *Clim. Change*, 43, 513-535,

Franzen, L.G., 1991: The changing frequency of gales on the Swedish west coast and its possible relation to the increased damage to coniferous forests of southern Sweden. *Int. J. Climatol.*, 11, 769-793.

Giorgio, F., 1990: Simulation of regional climate using a limited area model nested in a general circulation model. *J. Clim.*, 3: 941-963.

Giorgio, F., Brodeur, C.S., Bates, G.T., 1994: Regional climate change scenarios over the United States produced with a nested regional climate model. *J. Clim.*, 7: 375-399.

Henderson-Sellers A. & Robinson P.J., 1986: *Contemporary climatology*. Longman Scientific & Tecnical. New York. 439pp.

Heino, R., Brazdil, R., Forland, E., Tuomenvirta, H., Alexandersson, H., Beniston, M., Pfister, C., Rebetez, M., Rosenhagen, G., Rösner, S., Wibig, J., 1999: Progress in the study of climatic extremes in northern and central Europe. *Clim. Change*, 42: 151-181.

Hoskins, B.J., Valdes, P.J., 1990: On the existence of storm-tracks. *J. Atm. Sci.*, 47: 1854-1864.

IPCC, 1996: Climate change 1995: *The science of climate change*. University Press, Cambridge, 572 pp.

Jacobeit, J., Jönsson, P., Bärring, L., Beck, C., Ekström, M., 2001: Zonal indices for Europe 1780-1995 and running correlations with temperature. *Clim. Change*, 48: 219-241.

Johns, T.C., Carnell, R.E., Crossley, J.F., Gregory, J.M., Mitchell, J.F.B., Senior, C.A., Tett, S.F.B., Wood, R.A., 1997: The second Hadley centre coupled ocean-atmosphere GCM: model description, spinup and validation. *Clim. Dyn.*, 13: 103-134.

Jones, P.D., New, M., Parker, D.E., Martin, S., Rigor, I.G., 1999: Surface air temperature and its changes over the past 150 years. Rev. Geophys., 37: 173-199.

Jönsson P, Fortuniak K., 1995: Interdecadal variations of surface wind directions in Lund, southern Sweden, 1741-1990. *Int. J. Climatol.*, 15: 447-461.

Korevaar, C.G., 1990: *North Sea climate based on observations from ships and lightvessels*, Kluwer Academic Publishers, Netherlands. 137 pp.

Kushnir, Y., Cardone, V.J., Greenwood, J.G., Cane, M.A., 1997: The recent increase in North Atlantic wave heights. *J. Clim.*, 10: 2107-2113

Lambert, S.J., 1995: The effect of enhanced greenhouse warming on winter cyclone frequencies and strengths. *J. Clim.*, 8: 1447-1452.

Lau, N.C., 1988: Variability of the observed midlatitude storm tracks in relation to low-frequency changes in the circulation pattern. *J. Atm. Sci.*, 45: 2718-2743.

Lunkeit, F., Fraedrich, K., Bauer, S.E., 1998: Storm tracks in a warmer climate: sensitivity studies with a simplified global circulation model. *Clim. Dyn.*, 14: 813-826.

Munich Re, 2000: *Topics 2000 Natural catastrophes – the current position*. Munich Reinsurance Company, Germany. 126 pp.

Persson, A., 1998: How do we understand the Coriolis force? *Bull. Amer. Met. Soc.*, 79: 1373-1385.

Rummukainen, M., Räisänen, J., Ullerstig, A., Bringfelt, B., Hansson, U., Graham, P., Willén, U., 1998: RCA-Rossby Centre regional atmospheric climate model: model description and results from the first multi-year simulation. *SMHI Reports Meteorology and Climatology, No. 83*. 76 pp.

Schmidt, H., von Storch, H., 1993: German bight storms analyzed. *Nature*, 365: 791

Schmith, T., Kaas, E., Li, T.S., 1998: Northeast Atlantic winter storminess 1875-1995 re-analyzed. *Clim. Dyn.,* 14: 529-536.

Stull, R.B., 1995: *Meteorology today for scientists and engineers. A technical companion book.* West Publishing Company. St. Paul, Minnesota. 385 pp.

SWECLIM, 1998: Regional climate simulation for the Nordic region – First results from SWECLIM. SMHI, Norrköping. 22 pp.

Trenberth, K. E., 1997: The use and abuse of climate models. *Nature,* 386: 131-133.

Ulbrich, U., Christoph, M., 1999: A shift of the NAO and increasing storm track activity over Europe due to anthropogenic greenhouse gas forcing. Clim. Dyn., 15: 551-559.

von Storch, H., Reichartdt, H., 1997: A scenarioario of storm surge statistics for the German bight at the expected time of doubled atmospheric carbon dioxide concentration. *J. Clim.,* 10: 2653-2662.

The WASA Group, 1998: Changing waves and storms in the Northeast Atlantic? *Bull. Amer. Met. Soc.,* 79: 741-760.

Zhang, Y. Wang, W-C., 1997: Model-simulated northern winter cyclone and anticyclone activity under a greenhouse warming scenarioario. *J. Clim.,* 10: 1616-1634.

Zwiers, F.W., Kharin, V.V., 1998: Changes in the extremes of the climate simulated by CCC GCM2 under CO_2 doubling. *J. Clim.,* 11: 2200-2222.

Appendix I

Coordinates for the grid points of the two profiles through Sweden and the North Sea

	Profile through Sweden		Profile through North Sea	
Grid point	Long	Lat	Long	Lat
26	14.38°E	70.33°N	1.26°W	70.57°N
25	12.97°E	69.32°N	0.05°W	69.88°N
24	13.69°E	68.56°N	1.08°E	69.19°N
23	14.35°E	67.80°N	0.31°E	68.11°N
22	13.07°E	66.80°N	1.34°E	67.41°N
21	13.70°E	66.04°N	0.59°E	66.33°N
20	14.30°E	65.28°N	1.54°E	65.63°N
19	14.86°E	64.51°N	0.81°E	64.55°N
18	13.69°E	63.51°N	1.69°E	63.85°N
17	14.23°E	62.75°N	2.53°E	63.14°N
16	14.75°E	61.98°N	1.81°E	62.07°N
15	13.66°E	60.98°N	2.59°E	61.36°N
14	14.16°E	60.22°N	1.91°E	60.28°N
13	14.64°E	59.46°N	2.64°E	59.57°N
12	13.63°E	58.45°N	3.35°E	58.86°N
11	14.09°E	57.69°N	2.68°E	57.78°N
10	14.54°E	56.93°N	3.35°E	57.07°N
9	13.60°E	55.92°N	3.99°E	56.35°N
8	14.03°E	55.16°N	3.34°E	55.28°N
7	14.45°E	54.40°N	3.95°E	54.56°N
6	13.57°E	53.39°N	4.55°E	53.84°N
5	13.97°E	52.63°N	3.92°E	52.77°N
4	14.37°E	51.87°N	4.49°E	52.05°N
3	13.55°E	50.86°N	5.04°E	51.33°N
2	13.93°E	50.10°N	4.44°E	50.26°N
1	14.31°E	49.34°N	4.97°E	49.54°N

Lunds Universitets Naturgeografiska institution. Seminarieuppsatser. Uppsatserna finns tillgängliga på Naturgeografiska institutionens bibliotek, Sölvegatan 13, 223 62 LUND.

The reports are available at the Geo-Library, Department of Physical Geography, University of Lund, Sölvegatan 13, S-223 62 Lund, Sweden.

1. Pilesjö, P. (1985): Metoder för morfometrisk analys av kustområden.
2. Ahlström, K. & Bergman, A. (1986): Kartering av erosionskänsliga områden i Ringsjöbygden.
3. Huseid, A. (1986): Stormfällning och dess orsakssamband, Söderåsen, Skåne.
4. Sandstedt, P. & Wällstedt, B. (1986): Krankesjön under ytan - en naturgeografisk beskrivning.
5. Johansson, K. (1986): En lokalklimatisk temperaturstudie på Kungsmarken, öster om Lund.
6. Estgren, C. (1987): Isälvsstråket Djurfälla-Flädermo, norr om Motala.
7. Lindgren, E. & Runnström, M. (1987): En objektiv metod för att bestämma läplanteringars läverkan.
8. Hansson, R. (1987): Studie av frekvensstyrd filtringsmetod för att segmentera satellitbilder, med försök på Landsat TM-data över ett skogsområde i S. Norrland.
9. Matthiesen, N. & Snäll, M. (1988): Temperatur och himmelsexponering i gator: Resultat av mätningar i Malmö.

10A. Nilsson, S. (1988): Veberöd. En beskrivning av samhällets och bygdens utbyggnad och utveckling från början av 1800-talet till vår tid.

10B. Nilson, G., 1988: Isförhållande i södra Öresund.

11. Tunving, E. (1989): Översvämning i Murciaprovinsen, sydöstra Spanien, november 1987.
12. Glave, S. (1989): Termiska studier i Malmö med värmebilder och konventionell mätutrustning.
13. Mjölbo, Y. (1989): Landskapsförändringen - hur skall den övervakas?
14. Finnander, M-L. (1989): Vädrets betydelse för snöavsmältningen i Tarfaladalen.
15. Ardö, J. (1989): Samband mellan Landsat TM-data och skogliga beståndsdata på avdelningsnivå.
16. Mikaelsson, E. (1989): Byskeälvens dalgång inom Västerbottens län. Geomorfologisk karta, beskrivning och naturvärdesbedömning.
17. Nhilen, C. (1990): Bilavgaser i gatumiljö och deras beroende av vädret. Litteraturstudier och mätning med DOAS vid motortrafikled i Umeå.
18. Brasjö, C. (1990): Geometrisk korrektion av NOAA AVHRR-data.
19. Erlandsson, R. (1991): Vägbanetemperaturer i Lund.
20. Arheimer, B. (1991): Näringsläckage från åkermark inom Brååns dräneringsområde. Lokalisering och åtgärdsförslag.
21. Andersson, G. (1991): En studie av transversalmoräner i västra Småland.

22A. Skillius, Å., (1991): Water havesting in Bakul, Senegal.

22B. Persson, P. (1991): Satellitdata för övervakning av höstsådda rapsfält i Skåne.

23. Michelson, D. (1991): Land Use Mapping of theThat Luang - Salakham Wetland, Lao PDR, Using Landsat TM-Data.
24. Malmberg, U. (1991): En jämförelse mellan SPOT- och Landsatdata för vegetations-klassning i Småland.
25. Mossberg, M. & Pettersson, G. (1991): A Study of Infiltration Capacity in a Semiarid Environment, Mberengwa District, Zimbabwe.
26. Theander, T. (1992): Avfallsupplag i Malmöhus län. Dränering och miljö-

påverkan.
27. Osaengius, S. (1992): Stranderosion vid Löderups strandbad.
28. Olsson, K. (1992): Sea Ice Dynamics in Time and Space. Based on upward looking sonar, satellite images and a time series of digital ice charts.
29. Larsson, K. (1993): Gully Erosion from Road Drainage in the Kenyan Highlands. A Study of Aerial Photo Interpreted Factors.
30. Richardson, C. (1993): Nischbildningsprocesser - en fältstudie vid Passglaciären, Kebnekaise.
31. Martinsson, L. (1994): Detection of Forest Change in Sumava Mountains, Czech Republic Using Remotely Sensed Data.
32. Klintenberg, P. (1995): The Vegetation Distribution in the Kärkevagge Valley.
33. Hese, S. (1995): Forest Damage Assessment in the Black Triangle area using Landsat TM, MSS and Forest Inventory data.
34. Josefsson, T. och Mårtensson, I. (1995). A vegetation map and a Digital Elevation Model over the Kapp Linné area, Svalbard -with analyses of the vertical and horizontal distribution of the vegetation.
35. Brogaard, S och Falkenström, H. (1995). Assessing salinization, sand encroachment and expanding urban areas in the Nile Valley using Landsat MSS data.
36. Krantz, M. (1996): GIS som hjälpmedel vid växtskyddsrådgivning.
37. Lindegård, P. (1996). Vinterklimat och vårbakslag. Lufttemperatur och kådflödessjuka hos gran i södra Sverige.
38. Bremborg, P. (1996). Desertification mapping of Horqin Sandy Land, Inner Mongolia, by means of remote sensing.
39. Hellberg, J. (1996). Förändringsstudie av jordbrukslandskapet på Söderslätt 1938-1985.
40. Achberger, C. (1996): Quality and representability of mobile measurements for local climatological research.
41. Olsson, M. (1996): Extrema lufttryck i Europa och Skandinavien 1881-1995.
42. Sundberg, D. (1997): En GIS-tillämpad studie av vattenerosion i sydsvensk jordbruksmark.
43. Liljeberg, M. (1997): Klassning och statistisk separabilitetsanalys av marktäckningsklasser i Halland, analys av multivariata data Landsat TM och ERS-1 SAR.
44. Roos, E. (1997): Temperature Variations and Landscape Heterogeneity in two Swedish Agricultural Areas. An application of mobile measurements.
45. Arvidsson, P. (1997): Regional fördelning av skogsskador i förhållande till mängd SO_2 under vegetationsperioden i norra Tjeckien.
46. Akselsson, C. (1997): Kritisk belastning av aciditet för skogsmark i norra Tjeckien.
47. Carlsson, G. (1997): Turbulens och supraglacial meandring.
48. Jönsson, C. (1998): Multitemporala vegetationsstudier i nordöstra Kenya med AVHRR NDVI
49. Kolmert, S. (1998): Evaluation of a conceptual semi-distributed hydrological model – A case study of Hörbyån.
50. Persson, A. (1998): Kartering av markanvändning med meteorologisk satellitdata för förbättring av en atmosfärisk spridningsmodell.
51. Andersson, U. och Nilsson, D. (1998): Distributed hydrological modelling in a GIS perspective – an evaluation of the MIKE SHE model.
52. Andersson, K. och Carlstedt, J. (1998): Different GIS and remote sensing techniques for detection of changes in vegetation cover - A study in the Nam Ngum and Nam Lik catchment areas in the Lao PDR.

53. Andersson, J., (1999): Användning av global satllitdata för uppskattning av spannmålsproduktion i västafrikanska Sahel.
54. Flodmark, A.E., (1999): Urban Geographic Information Systems, The City of Berkeley Pilot GIS
55A. Lyborg, Jessic & Thurfell, Lilian (1999): Forest damage, water flow and digital elevation models: a case study of the Krkonose National Park, Czech Republic.
55B. Tagesson, I., och Wramneby, A., (1999): Kväveläckage inom Tolångaåns dräneringsområde – modellering och åtgärdssimulering.
56. Almkvist, E., (1999): Högfrekventa tryckvariationer under de senaste århundradena.
57. Alstorp, P., och Johansson, T., (1999): Översiktlig buller- och luftföroreningsinventering i Burlövs Kommun år 1994 med hjälp av geografiska informationssystem – möjligheter och begränsningar.
58. Mattsson, F., (1999): Analys av molnklotter med IRST-data inom det termala infraröda våglängdsområdet
59. Hallgren, L., och Johansson, A., (1999): Analysing land cover changes in the Caprivi Strip, Namibia, using Landsat TM and Spot XS imagery.
60. Granhäll, T., (1999): Aerosolers dygnsvariationer och långväga transporter.
61. Kjellander, C., (1999): Variations in the energy budget above growing wheat and barley, Ilstorp 1998 - a gradient-profile approach
62. Moskvitina, M., (1999): GIS as a Tool for Environmental Impact Assessment - A case study of EIA implementation for the road building project in Strömstad, Sweden
63. Eriksson, H., (1999): Undersökning av sambandet mellan strålningstemperatur och NDVI i Sahel.
64. Elmqvist, B., Lundström, J., (2000): The utility of NOAA AVHRR data for vegetation studies in semi-arid regions.
65. Wickberg, J., (2000): GIS och statistik vid dräneringsområdesvis kväveläckagebeskrivning i Halland.
66. Johansson, M., (2000): Climate conditions required for re-glaciation of cirques in Rassepautasjtjåkka massif, northern Sweden.
67. Asserup, P., Eklöf, M., (2000): Estimation of the soil moisture distribution in the Tamne River Basin, Upper East Region, Ghana.
68. Thern, J., (2000): Markvattenhalt och temperatur i sandig jordbruksmark vid Ilstorp, centrala Skåne: en mätnings- och modelleringsstudie.
69. Andersson, C., Lagerström, M., (2000): Nitrogen leakage from different land use types - a comparison between the watersheds of Graisupis and Vardas, Lithuania.
70. Svensson, M., (2000): Miljökonsekvensbeskrivning med stöd av Geografiska Informationssystem (GIS) – Bullerstudie kring Malmö-Sturup Flygplats.
71. Hyltén, H.A., Uggla, E., (2000): Rule.Based Land Cover Classification and Erosion Risk Assessment of the Krkonoše National Park, Czech Republic.
72. Cronquist, L., Elg, S., (2000): The usefulness of coarse resolution satellite sensor data for identification of biomes in Kenya.
73. Rasmusson, A-K., (2000): En studie av landskapsindex för kvantifiering av rumsliga landskapsmönster.
74. Olofsson, P., Stenström, R., (2000): Estimation of leaf area index in southern Sweden with optimal modelling and Landsat 7 ETM+Scene.
75. Uggla, H., (2000): En analys av nattliga koldioxidflöden i en boreal barrskog avseende spatial och temporal variation.
76. Andersson, E., Andersson, S., (2000): Modellering och uppmätta kväveflöden i

energiskog som bevattnas med avloppsvatten.
77. Dawidson, E., Nilsson, C., (2000): Soil Organic Carbon in Upper East Region, Ghana - Measurements and Modelling.
78. Bengtsson, M., (2000): Vattensänkningar - en analys av orsaker och effekter.
79. Ullman, M., (2001): El Niño Southern Oscillation och dess atmosfäriska fjärrpåverkan.